Monitoring Rainwater Harvesting Systems in India Using Satellite Remote Sensing Observations

by

Vicky Vanthof

A thesis
presented to the University of Waterloo
in the fulfilment of the
thesis requirement for the degree of
Master of Science
in
Geography

Waterloo, Ontario, Canada, 2018

I hereby declare that I am the sole author of this thesis. This is a true copy of the thesis, including any required final revisions, as accepted by my examiners.

I understand that my thesis may be made electronically available to the public.

Abstract

The building of small reservoirs is a typical measure taken by farmers to moderate the extremes of the hydrologic regime of a semiarid climate, which is characterized by the alternation of a short rainy season with long periods of dryness. South India is an example of a region that has utilized ancient village-level small rainwater harvesting (RWH) reservoirs (also known as tanks) for seasonal water storage. Decades of increasing dependence on groundwater has caused these tanks to fall into a state of disrepair. Now the severity of depleted groundwater resources is driving renewed efforts at the state and national levels to revive RWH systems. Critical to the success of the revival efforts and tank management is the regular monitoring of the water volume variations. Although synthetic aperture radar (SAR) observations have long been recognized as an important source of remote sensing (RS) data for monitoring surface water (SW) under all-weather conditions, and is used operationally for SW mapping applications, limited information is available about the limits of SAR RS technologies for small reservoirs for irrigation purposes.

This thesis describes a RS approach to water volume monitoring in small reservoirs (5-80 ha in size) in the Gundar river basin, Tamil Nadu state in S. India. Empirically-derived water storage relationships were evaluated using TanDEM-X digital elevation model (DEM) data combined with estimates of SW extent from C-band Sentinel-1A (S1-A) SAR observations, and Landsat-8, Sentinel-2, and PlanetScope visible/infra-red observations. The TanDEM-X DEM data revealed strong power-type relationships between SW extent and storage volume, and were combined with satellite SW observations to estimate and monitor tank volumes. Three models of volume-area (V–A) relationship(s) were assessed: a tank specific (TS) model, a size-dependent categorical (CAT) model and a generalized (GEN) model for all tanks. For volume estimation, the CAT model produced the lowest root mean squared error (RMSE) as a percentage, V_{ERR}, of volume for the basin. While tank SW area was estimated using S-1A data, the narrow SW area of some tanks, especially close to the retaining wall presented challenges for operational use. Two examples demonstrate the approach: 1) the maximum volume of water in 559 tanks in the basin for two monsoon seasons shows tank structures significantly under-performing and 2) a time-series analysis using a high-volume of satellite observations shows the cycle of water (inflow and outflow) at the tank scale.

This thesis illustrates the applicability of using a satellite RS observation approach to continuously monitor RWH, and beyond this, the critical need of an adopted multi-sensor approach (optical and radar) to retrieve high spatio-temporal resolution monitoring. The ability to estimate reservoir volumes using satellite RS has wide reaching implications in transboundary water management. RWH tank systems are currently not continuously monitored and thus, our findings represent a unique contribution to the hydrologic science community by illustrating the applicability of using a satellite RS observation approach to monitor RWH structures during monsoon, habitually cloud-covered, seasons.

Acknowledgements

Through the course of this work I have been fortunate to have the support and guidance of many. First, thank you to my supervisor, Dr. Richard Kelly, for giving me guidance and the academic freedom to explore while not straying too far from my research goals. The fieldwork portion of my study was a key example of this freedom. Beyond this, travelling to the Northwest Territories (NWT) to help Aaron Thompson with his field research and participating in an ERASMUS research exchange to Friedrich Schiller University Jena in Germany are both unforgettable experiences that I am extremely grateful for. Words cannot express my appreciation for your guidance, patience, and understanding throughout this process. Also, thank you to Dr. Alexander Brenning for your guidance on both my thesis work and advice when adjusting to a new culture. I would also like to add my sincere thanks to my thesis committee members Dr. Nandita Basu, Dr. John Beebe and Dr. Claude Duguay.

I thank the DHAN Foundation for generously sharing their experiences and hospitality during our field visit that allowed for this project to be carried out. Help from Alwish Ranjith John Gnanaraj and Shaik Fareeth in the field was also most appreciated. I thank Planet and their Education and Research program for access to a great dataset of daily optical PlanetScope satellite observations. Likewise, I thank DLR (German Aerospace Centre) for providing access to the TanDEM-X DEM dataset under TanDEM-X Science Proposal DEM_HYDR075, which was crucial for tank volume estimation. I am additionally grateful for the financial support of the Ontario Graduate Scholarship Program and Natural Sciences and Engineering Research Council of Canada.

Friends and family have also been invaluable in helping me have fun and stay focused while working on my thesis. A special thank you goes to my fellow geographers: Aaron Thompson**,** Nastaran Saberi**,** Qinghuan Li**,** Margot Flemming**,** Paul Donchenko, Hongjing Chen and Peter Wray**.** Aaron Thompson, even though it was mentally and physically challenging, thank you for choosing me to work with you in the NWT because it was truly a once in a lifetime experience that I will never forget. ‘Morag’, thank you for being an awesome companion in Germany and I am grateful to have you as a friend. Finally, I thank my family, my boyfriend, and his family for their support through what has been an amazing but challenging process. Your continued support pushed me to the finish line.

Table of Contents

List of Figures

List of Tables

Preface

The thesis presented here has been formatted according to the University of Waterloo's Guidelines for the Manuscript Option, Masters in Geography. Chapter 3 represents a manuscript submitted to *Remote Sensing of Environment*.

> Vanthof V and REJ Kelly (2018). Estimating seasonal surface water storage in rainwater harvesting reservoirs in southeast India using satellite remote sensing.

The research presented here was conducted and written by V. Vanthof, and was made possible by the guidance and assistance of Professor R.E.J. Kelly. A preliminary version of Chapter 3 was presented by oral presentations at a refereed conference: Vanthof & Kelly (2018).

> V. R. Vanthof and R. E. J. Kelly, "Rainwater harvesting in India: Using Radar remote sensing observations to monitor water storage," in Proceedings of the *2018 IEEE International Geoscience and Remote Sensing Symposium (IGARSS)*, Valencia, Spain, 2018.

Chapter 1

General Introduction

The availability of freshwater resources in the form of lakes, reservoirs, groundwater and river systems are critical for terrestrial life and ecosystem services. Only 2.5 % of the world's total water supply is freshwater and only 29.9 % and 0.26 % of the total freshwater represent groundwater resources and surface waters stores respectively (Degefu, Weijun, Zaiyi, Liang, & Zhengwei, 2018; Shiklomanov, 2000). Global freshwater availability and variability has been linked to a variety of stressors influenced by human, climatic, and physiographic factors (Kummu et al., 2016; Vorosmarty, Green, Salisbury, & Lammers, 2000). These stressors have increased water demand and placed increased pressure on variable and unpredictable freshwater resources. Numerous lines of evidence suggest that water shortages and water scarcity will be one of the world's greatest challenges in the 21st century (Kummu et al., 2016; Vorosmarty et al., 2000; Wada et al., 2010).

1.1 Motivation

In India, like many countries in semi-arid climatic zones, water stress for human activities is driven not only by population increases, changes in food consumption, and climate driven changes in water availability (Wiltshire et al., 2013), but also by spatial and temporal differences between water availability and water demand (Degefu et al., 2018). In semi-arid regions where rainfall variability is high, some communities have developed adaptation strategies to deal with climatic variability by building rainwater harvesting (RWH) structures. Characterized by both spatial and temporal mismatches in water stress and availability, the climatic regime of South India is one such example of a region that has developed RWH structures. Across S. India are thousands

of human-made reservoirs (known as tanks), the construction of which date back 2000 years (Kumar, Patel, Ravindranath, & Singh, 2008). A tank is an ancient engineered structure designed at the localized scale with earthen embankments to store water for later use. Often arranged in cascading systems with a single tank serving one village, these tanks were developed as a strategy for managing the seasonal and inter-annual rainfall variability (Kumar et al., 2008). However, the underuse of these systems in recent decades, and the over extraction of groundwater, has caused many tanks to fall into a state of disrepair (Appendix A).

Evaluating the rehabilitation of these structures and their re-emerging use for an effective mitigation measure against climate extremes has generated a significant amount of literature from non-governmental organizations (NGOs), scientists and public health specialists around the world (Gunnell & Krishnamurthy, 2003; Kumar & Rao, 2017; Kumar et al., 2013; Sakthivadivel, Fernando, & Brewer, 1997; Shah, 2004). This literature questions whether these systems, developed decades ago during a very different climatic regime, still serve their intended purpose in the Anthropocene. While recent efforts have contributed to a revival of RWH structures, there still exists a significant knowledge gap regarding the volume variation of water within these systems.

Quantifying variations in tank water volumes is not possible from conventional ground based stage measurements in S. India because it is estimated that more than 120,000 RWH tanks exist (Gunnell & Krishnamurthy, 2003). The availability of remotely sensed data and image processing techniques offers a potential cost and time effective means of monitoring water volume changes in tank systems which is of significant use for farming communities in this region.

1.2 Aims and objectives

The overall intent of this thesis is to provide a better understanding about how remote sensing (RS) observations can contribute to a greater understanding of the hydrology, and particularly water volume dynamics of RWH tank systems. Given the limited RS observation-based studies of tanks in S. India and the importance of such observations as an intermediary to increased understanding of tank water dynamics, this thesis attempts to answer the question: can a remotely-sensed observation framework be developed to monitor the surface water storage (SWS) of tank systems? Developed in this thesis, the tank water volume space-based approach combines a novel high-precision global digital elevation model (DEM) to derive simple empirical models with the fusion of a dense time-series of repeat pass synthetic aperture radar (SAR) observations and high resolution multispectral visible infrared PlanetScope (PS), Sentinel-2A (S2) and Landsat-8 (L8) satellite observations.

This study has three closely related sub-objectives concurrent to developing a tank water volume space-based monitoring approach: (1) evaluate the applicability of the new novel TanDEM-X DEM for the accurate retrieval of tank bathymetry, (2) evaluate the suitability of empirical power models to quantify tank water volume at three levels – tank specific (TS) level, a clustered categorical (CAT) level, and a generalized (GEN) level, and (3) demonstrate the suitability of volume estimation using surface water (SW) extent extracted from a dense archive of freely available RS space-based radar and optical observations. Cumulatively, the former sub-objectives will provide an understanding as to the degree to which space-based volume estimates can inform mass water balance components, given the current and future earth observation (EO) data climate, and contribute a greater understanding to tank hydrology. This thesis provides the first step required to evaluate and provide understanding for the availability of water in tanks

systems at large spatial scales. This monitoring is crucial for the understanding and characterization of water mass balance dynamics in these RWH systems and have applicability in other regions of the world.

1.3 Motivation of research

The Indian population is expected to increase by 450 million, one-third more than at present by 2050. This increase in population along with projected increase in average annual temperature by 2 degrees Celsius by 2050 for South Asia (Hijioka et al., 2014), and increasingly sporadic monsoon periods in S. India (Hijioka et al., 2014; Karmakar, Chakraborty, & Nanjundiah, 2017), highlights the need to better understand the usage of tank systems to mitigate against climate extremes. Given the expected increase in population and changes in climate, livelihood's in India will continue to face challenges surrounding water availability. For S. India, a region where agriculture is primarily rain fed and groundwater irrigation is no longer sustainable, the rehabilitation of SW stores in the form of tanks is of critical importance to improve future water management.

The usage of RS data to understand tanks is key to provide information over large spatial scales and for inaccessible locations. This information can equip policy makers and scientists with tools to evaluate the impact of tanks on the water budget. The goal is to use near real-time RS data to better inform resource management decisions, by providing water allocation estimates for irrigation based on current hydrological conditions, as opposed to a fixed amounts or knowledge based on the modelling of historical data. The presented research seeks to provide a method for monitoring water volume in tank systems in S. India with potential applicability to other regions with similar water issues.

1.4 Structure of thesis

This thesis has been written following the manuscript structure in which a standalone paper is included as a separate chapter. Chapter 2 provides background information on tank structure, water balance components and the influence of climate change as well as a review on RS of inland water body monitoring, with a focus on SAR. Chapter 3 is the appended paper, entitled "Estimating seasonal surface water storage in rainwater harvesting reservoirs in southeast India using satellite remote sensing". Chapter 4 identifies the limitations of the study, and lists recommendations for future studies utilizing RS observations to contribute greater understanding of tank systems. Chapter 5 provides a conclusion.

1.5 Appended paper synopsis

To monitor water volume changes in tanks, empirical volume-area (V-A) relationships were developed for a large subset of tanks (n=72) using a global DEM product and subsequently combined with SW extent extracted from a series of visible/infra-red and SAR satellite scenes. While studies have implemented empirical equations to approximate reservoir bathymetry in other semi-arid environments (Annor et al., 2009; Liebe, Giesen, Andreini, Steenhuis, & Walter, 2009; Sawunyama, Senzanje, & Mhizha, 2006), no work has focused on water volume estimation for tanks in S. India. Furthermore, in the context of continuously monitoring RWH tanks, neither the SAR techniques nor the implementation of a high-resolution global DEM to evaluate water storage has been performed previously.

Chapter 2

Background and Literature Review

In this chapter background context relevant to the study is presented before a literature review on tank SWS using RS space-based observations. Background information includes a description of the study area and detail on SWS structures and groundwater irrigation in S. India. Further discussion follows regarding changing climate implications, the physical structure of tanks and their water balance, and finally the current approaches used to understand tank systems. The literature review focuses on the methods available to measure SWS of reservoirs, with a focus on SAR, and concludes by outlining how the former discussed methods can apply for RWH structures in S. India.

2.1 Study region and context

The Gundar river basin (5647 km^2) in the S. Indian state of Tamil Nadu (Figure 2.1a) is a river basin with a large concentration of small seasonal water storage reservoir structures and was selected for the specific study region. Figure 2.1a highlights the spatial extent of tanks across the state of Tamil Nadu, occupying 1.61 % of the state area, as captured from a global surface water (GSW) dataset (n= 36,575) (Pekel, Cottam, Gorelick, & Belward, 2016). The basin has a semi-arid climate which is characterized by two two-month, monomodal monsoon climate seasons and an average rainfall of 770 mm per year.

The Gundar is referred to as a "monsoon shadow area" (Sato, 2017), where peak rainfall is not observed during the typical southwest monsoon (SWM) period (June–September) but rather during the dryer northeast monsoon (NEM) season (October–December) (Figure 2.2). For

agriculture in the region, while total annual rainfall is important, the timing and intensity during the monsoon season is equally important. Figure 2.2 shows mean estimated precipitation for the Gundar from 1981–present and highlights that each year the NEM provides most of the annual precipitation, whereas precipitation from the SWM and other months are minimal in comparison (Funk et al., 2015). Also, the SWM and NEM precipitation patterns are spatially heterogeneous across the Gundar, with the upper basin experiencing higher precipitation levels during the NEM than the lower basin, and the opposite for the SWM. For centuries, this precipitation regime has enabled farmers to rely on small storage reservoirs, which often are the only source of water available for dry-season crops. During the NEM season, rice is the primary crop, while cotton, groundnuts and a variety of pulses are cultivated during other periods of the year (Van Meter, Steiff, McLaughlin, & Basu, 2016). This productivity is sustained in the basin by an estimated 2314 tanks in combination with groundwater pumping.

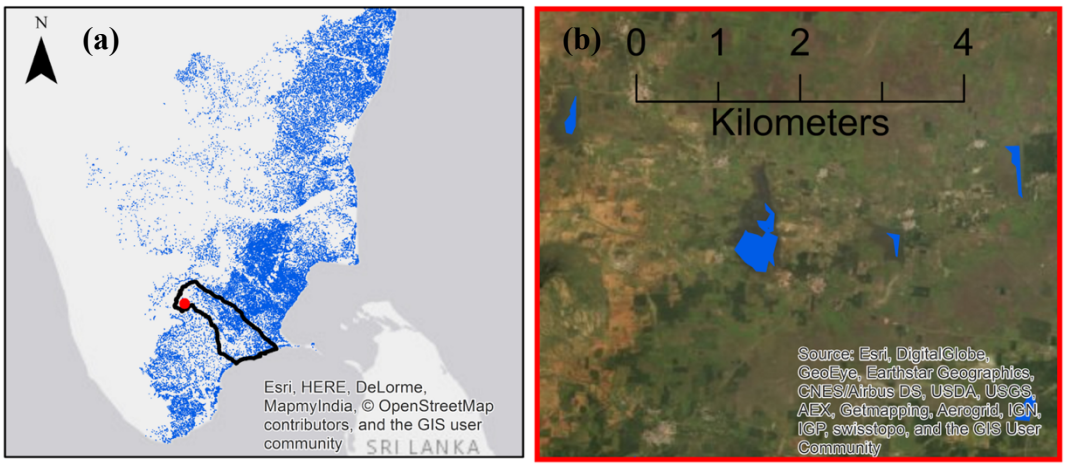

Figure 2.1: Location of the Gundar River Basin. (a) Distribution of tanks across Tamil Nadu identified from the GSW dataset. (b) Upper Gundar field data site visited June 2016.

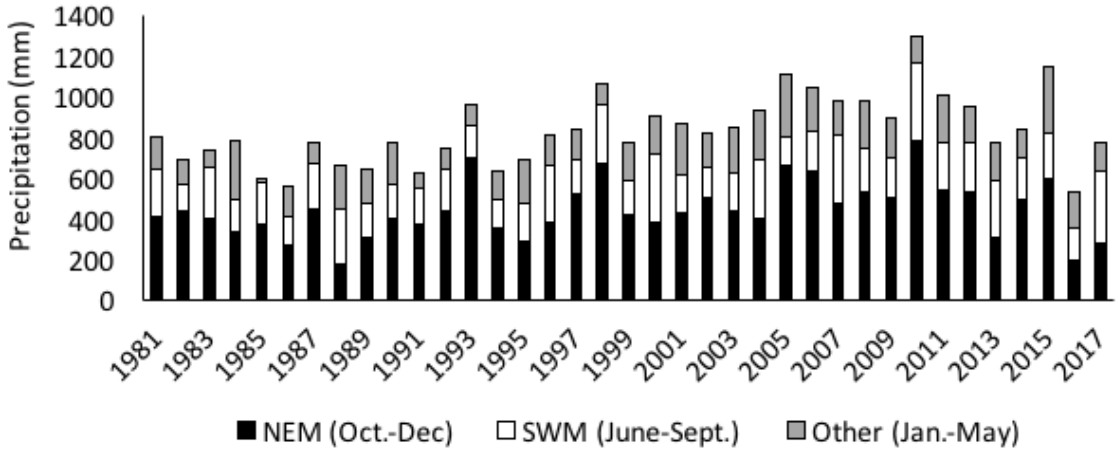

Figure 2.2: Yearly precipitation in the Gundar River Basin separated by the two distinct monsoon seasons and the other months. Data calculated from Climate Hazards Group InfraRed Precipitation with Station data gridded rainfall product (Funk et al., 2015).

2.2 Small reservoir irrigation tanks

Small reservoirs are known under multiple names in various regions of the world: tanks or johads in South Asia, açudes in Brazil, small reservoirs or micro-dams in sub-Saharan Africa, and lacs collinaires in North Africa. Also, the definition of a small reservoir is not agreed upon. Here the generic term 'small reservoirs' or 'tanks' is used to define small reservoirs as reservoirs with a surface area smaller than 100 ha.

Small seasonal water storage reservoir structures are an indispensable part of rural village life in S. India. They can be found across the S. Indian landscape with some being thousands of millennia old (dating back to 2600 BC) and can typically be described as small man-made reservoir structures developed using earthen banks across natural depressions in the landscape (D. Kumar et al., 2008; Pandey, Gupta, & Anderson, 2003). Tanks shape the landscape from their dense distribution; 159,000 and 39,000 in S. India and Tamil Nadu respectively servicing 65,000 and 15,000 villages (Aubriot & Prabhakar, 2011). Historically, the primary purpose of these ancient structures was to alleviate periods of water shortages by storing water that can be harvested during

the monsoon and the subsequent dry season. These systems were vital for farmers to make decisions regarding when, what, and how much to plant.

Dependence on SW for irrigation has been overtaken by the extensive use of groundwater in the region (Kajisa, Palanisami, & Sakurai, 2007; D. Kumar et al., 2008; Van Meter et al., 2016). Until the 1950s, tank irrigation was a sustainable strategy to cope with rainfall variability, providing irrigation to over 20 % of the cropped area in the S. Indian states. Historically, although these systems provided an indispensable water supply capable of sustaining the socioecological balance of the village ecosystem, many tanks have fallen into a state of disrepair and have become defunct. While the reasons for the decline in tank functionality are multifaceted and include an array of political, social, physical, and economic factors (Bitterman, Tate, Van Meter, & Basu, 2016; Kajisa et al., 2007; Kumar & Rao, 2017; Mosse, 2018), the introduction of private groundwater wells with the onset of the Green Revolution in the 1960s has caused the significance of tanks as collective water resource system to greatly diminish.

Before the Green Revolution, India was a minor consumer of groundwater for agricultural irrigation compared to other countries. This has drastically changed; from 2000 onwards, India has extracted more groundwater than any other country in the world, accounting for 25 % of the worlds extracted groundwater (Shah, 2004, 2009) (Figure 2.3). The Green Revolution, combined with new pump technology and cheap rural electrification, led to a 130-fold increase in irrigation wells across India, from 0.15 million in 1960 to nearly 20 million by 2000 (Sishodia, Shukla, Graham, Wani, & Garg, 2016). While groundwater irrigation has driven the development of India's agriculture economy by increasing yields and productivity (leading to improved livelihoods), the scale of groundwater development and reliance has caused severe groundwater depletion and degradation. For the southern state of Tamil Nadu, groundwater extraction now exceeds 100 % of

the natural groundwater recharge for several districts. As a result, one third of the states' groundwater resources are identified as over exploited (Government of Tamil Nadu, 2015). The increase in groundwater extraction and the decline in the use of SW for irrigation has occurred concurrently. The ratio of tank irrigated area in India has decreased from 16 % in 1952-53 to 5 % in 1999-2000, whereas the ratio of well irrigated area has increased from 30 % to 55 % for the same period (Palanisami et al., 2010).

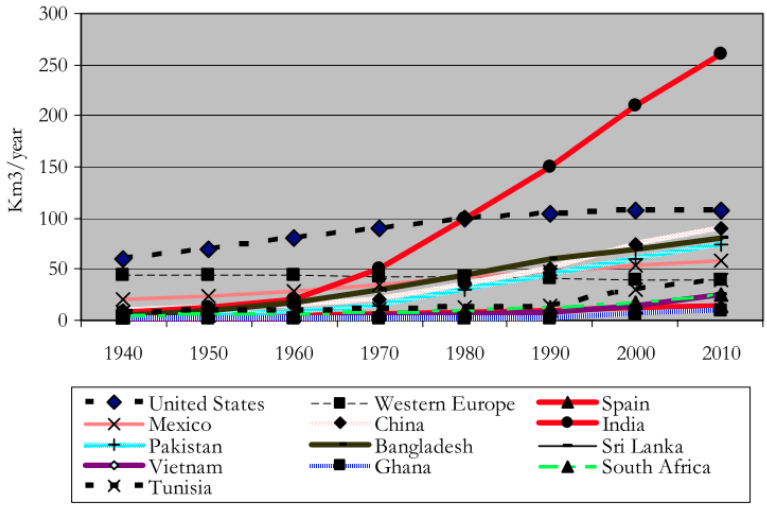

Figure 2.3: Growth in agricultural groundwater use in selected countries: 1940–2010. Source (Shah, 2004, 2009)

The impact of decline in the use of tank structures on the rural communities is multi-facetted. Apart from irrigation and domestic use, tanks serve a variety of purposes with applications to forestry, fisheries and brick-making (Kumar & Rao, 2017). Furthermore, the shift from tank to groundwater as the dominant source of irrigation has directly impacted inequality and poverty (Gunnell & Krishnamurthy, 2003; Kajisa et al., 2007). In theory, access to water from tank irrigation was available to all farmers in the command area through an equitable management system. However, when water reliance shifted away from tank irrigation to private wells, water became limited to the owners of the wells or those who can afford to buy from the owners. A study

on changing farming practices in Tamil Nadu found that there was a reduction in both crop yield and income for tank dependent farmers, causing a growth in the more reliable water source of well irrigation that subsequently produced an increased deterioration in tank performance (Kajisa et al., 2007). This highlights that a well-functioning tank is directly linked with income, and is particularly important for the small, marginalized farmers whose livelihood is heavily dependent on tank water supply. Unfortunately, the continued depletion of groundwater is not a sustainable means of irrigation and as a result, village level RWH structures are being rehabilitated and re-evaluated as a promising solution to facilitate groundwater replenishment and recharge and for SW storage for later use (Government of Tamil Nadu, 2015).

2.3 Climate, forecasted changes, and livelihoods

The effort and interest in tank rehabilitation in recent years is driven by the knowledge that the livelihoods of rural S. Indian farmers, under current and future stressors (non-climate and climate-driven), are heavily threatened by the lack of water availability. Stressors refers not only to climate-induced stressors but also to rapid growth in population, increased agricultural need and industrial growth; all the former increase the demand for freshwater (Lele, Srinivasan, Thomas, & Jamwal, 2018). Groundwater, a resource which is declining rapidly, is the main source of irrigation for S. Indian agriculture (Kumar & Rao, 2017). Moving forward, re-introducing and utilizing local SW structures and protecting groundwater from further unsustainable declines should be a priority.

The impact of climate change on the availability of water resources in S. India is heavily documented (Lele et al., 2018; Mall, Gupta, Singh, Singh, & Rathore, 2006; Pandey et al., 2003; Siderius et al., 2015). According to the Intergovernmental Panel on Climate Change (IPCC) climate change scenarios, S. India will likely be affected by rising temperatures, a higher variability of monsoonal rainfall and an increase in climatic extreme events such as floods and

droughts (IPCC, 2014). These developments have potential to affect the future sustainable functionality and management of RWH structures to an unknown extent. Hence water storage to conserve rainwater due to climate change will gain more importance in the future (Siderius et al., 2015). The state of Tamil Nadu is of particular concern because the state is fully dependent on monsoon-rains for recharging its water resources and over 50 % of agricultural land requires irrigation (Government of Tamil Nadu, 2015).

2.4 Tank structure and water balance

A two-dimensional profile of typical geometry and topography of a tank structure found in S. India is shown in Figure 2.4. While this is only a single tank, each tank system is connected to the next in cascades with overflow from upstream tanks feeding downstream tanks or waterways. During monsoon rains, precipitation and runoff from the tank catchment area inundates the immediate tank area. Historically, sluices were constructed within the tank bund (retaining wall) and opened for water to route from the tank into irrigation channels and after to fields downstream in the command area (*i.e.*, tank-supported irrigated fields). Wells are also often present within the command area to supplement tank irrigation and are recharged annually by water from the tank (Glendenning & Vervoort, 2010). When the water level in the immediate tank area falls below the sluice channel, this water is referred to as ‘dead storage’ and contributes primarily to groundwater recharge and evaporation (Van Meter et al., 2016).

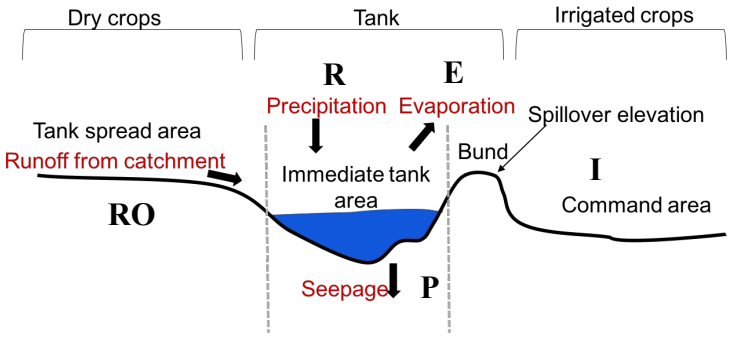

Figure 2.4: Schematic diagram of tank structure with tank components and mass balance variables described in Eq. (2.1).

Studies reported in the literature have shown that tank rehabilitation not only increases tank storage and in turn irrigation potential, but that rehabilitation heavily supports groundwater replenishment. In Tamil Nadu, it was observed that tanks help to increase the recharge by 40 percent (Van Meter et al., 2016). In the absence of tanks, especially in low rainfall years, water levels in the wells drastically drop. Furthermore, if tanks are present but do not receive adequate supplies of rainfall, well recharge is relatively small (Srivastava et al., 2009). Therefore, the loss of tank capacity correlates to a loss of groundwater recharge in tank dominated landscapes. Despite this, tank rehabilitation and the associated positive impacts on rural livelihoods and water availability is still in its infancy. Centuries ago when tanks were successfully utilized for water surface storage and groundwater recharge, the cropping dynamics, political structure and groundwater levels were quite different. It was unknown how efficient these structures were for serving their intended irrigation purpose. Therefore, to better understand the tank water storage dynamics, scientifically-driven information on tank water availability is necessary. This should include knowledge of the spatial and temporal changes of the water mass balance variables.

A tank's water balance can be expressed in equation (2.1) as follows:

$$\Delta V = (R_t + RO_t) - (I_t + P_t + E_t) \qquad (2.1)$$

where R is rainfall (m^3), RO is the surface runoff entering into tank (m^3), I is water used for supplemental irrigation (m^3), P *is* water percolating down to the groundwater table (m^3), and E *is* water lost due to evaporation (m^3). Together the former variables result in water volume changes ΔV (m^3) occurring between each time step (t).

Quantifying the incoming and outgoing fluxes requires hydrological modeling and/or *in situ* data, which, in turn, depends on the availability of meteorological variables. In ungauged basins, hydro-meteorological information is often unavailable and, therefore, hinders the ability to quantify basin-wide V or ΔV. Fortunately, in the last two decades, satellite RS has played an increasingly important role in water balance studies and has helped our understanding of, and ability to recover, water balance components (McCabe et al., 2017; McCabe et al., 2008). Quantifying V provides insight into water availability for downstream users (both in the command area and lower basin cascades) and helps to inform agricultural decisions, especially when and how much to plant. Furthermore, focusing on ΔV at the tank level over a large spatial area may provide understanding of geographic patterns in water release practices, variability in social rules, and cropping pattern influences; all information critical to the success of tank rehabilitation but extremely difficult to retrieve. Former hydrological modeling studies focusing on the hydrology and water mass balance dynamics of RWH tanks focus often on one or few tanks structures. Such studies utilize a range of local-scale environmental data that are often unavailable in many regions of the world (Glendenning & Vervoort, 2011; Li & Gowing, 2005; Van Meter et al., 2016). The former noted works and others are critical for the evaluation of understanding the successfully rehabilitation of tanks because tank dynamics are reliant on an array of complicated and diverse social, political, economic, and hydrological components. Despite such importance, the former studies are limited in their ability to gain breadth of knowledge into tank dynamics and therefore,

RS space-based observations can complement the former literature. Furthermore, RS space-based observations could potentially offer insight into local-scale environmental data required for tank hydrological modeling studies and a methodology that is analytically transparent and reproducible with potential for use in other settings around the world.

2.5 Estimating surface water storage (SWS) from remote sensing

Remotely sensed data can reinforce the abilities of water resources researchers and decision makers to monitor waterbodies more effectively by covering larger areas more cost effectively. Furthermore, RS techniques have been implemented widely to retrieve SW parameters (*e.g.*, water level, elevation, water extent). Although there are many RS satellites measuring water surfaces, there is no single sensor that can directly measure SWS. Instead, SWS and storage variations must be inferred from a combination of elevation (bathymetry or water height) and/or SW extent or area (A) estimates (Amitrano et al., 2014; Baup, Frappart, & Maubant, 2014; Crétaux et al., 2011; Crétaux & Birkett, 2006; Gao, Birkett, & Lettenmaier, 2012; Hong, Wdowinski, Kim, & Won, 2010; Medina, Gomez-Enri, Alonso, & Villares, 2010). Retrieval of the former parameters becomes increasing more difficult as the size of the waterbody decreases and as data scarcity limitations in regions are introduced. Here, a review is provided of the satellite RS approaches for SWS estimation. Remotely sensed estimation of SWS in a reservoir is possible via two methods: (1) satellite observations alone or (2) the combination of satellite observations and bathymetric information (Table 2.1).

Table 2.1: Methods for reservoir storage estimation. Sat = satellite image, Alt = altimetry data.

Type		Data		
Satellite observations alone				
(1)	a	A (Sat)	+	H (Alt)
	b	A (Sat)	→	H-A curve
	c	H (Alt)	→	H-A curve
Combination of satellite observations and a DEM				
(2)	d	A (Sat)	→	A-V curve (DEM)
	e	H (Alt)	→	H-V curve (DEM)
	f	A (Sat)	→	H-A curve (DEM)
	g	H (Alt)	→	H-A curve (DEM)

For type 1, deriving SWS exclusively from satellite observations, the first approach (a) requires a pair of satellite images and altimeter data observed at the same periods, and ΔV is calculated. Methods b and c provide ΔV from the water level (H) and A (*e.g.*, H-A curve), which is estimated by satellite observations, and satellite observed H or A. For methods b and c, once the empirical relationships are developed, SWS can be estimated if either satellite observations for A or altimeter data for H is obtained.

Unlike the method above, type 2 methods (d-g) require topographic data, based on a three-dimensional representation of the surface (*e.g.*, DEM), in addition to satellite observations. In these methods, empirical relationships are developed from the DEM, and combined with satellite observations of H or A to provide ΔV. Often satellite observations cannot be obtained due to a coarse spatial resolution (for the altimeter) or cloudiness (for visible and near-infrared sensors). If a good quality DEM is available, the Type 2 method allows the estimation of SWS with either satellite images for A or altimeter data for H.

2.5.1 Measurement of water level or height (H)

Satellite altimetry, originally developed to measure ocean surface topography (Brown, 1977) has been successfully applied to measure the variation of H in lakes (Crétaux et al., 2011; Crétaux & Birkett, 2006; Medina et al., 2010), rivers (Birkett, Mertes, Dunne, Costa, & Jasinski, 2002; Santos et al., 2012) and floodplains (Frappart, Seyler, Martinez, León, & Cazenave, 2005). Satellite radar altimetry is a system that measures the return time for a radar pulse to travel from the satellite antenna to the ground and back. By knowing the speed at which light travels, the time can be translated into a distance measurement (Medina et al., 2010). Despite the widespread use of satellite altimetry, the former studies highlight that achieving accurate H readings is a challenging task and the accuracy of H can vary substantially (from 5–80 cm). This variation is dependent on the type and spatial coverage of the altimetry sensor (*e.g*., from ERS-2 to Jason-2), the size of the water bodies being monitored, the configuration of the terrain, and the dominance of vegetation (Birkett et al., 2002; Crétaux et al., 2011; Crétaux & Birkett, 2006; Frappart et al., 2005; Medina et al., 2010; Santos et al., 2012). Focusing on the accuracy of H as a function of size, early work showed that radar altimetry was successfully used for monitoring large rivers with widths greater than 1 km (Birkett et al., 2002; Birkett, 1998). Until recently, few studies have focused on the limits of the RS altimetry technologies applied to small lakes and reservoirs. With the advancement of re-tracker algorithms, recent studies demonstrate the success of H retrieval for small rivers (< 100 m width) and small reservoirs (< 100 ha) (Baup et al., 2014; Kuo & Kao, 2011). Compared to the size of the rivers or the water bodies in the above-mentioned studies, most tanks have significantly smaller immediate tank areas (2–20 ha). In addition, a major drawback is the poor density of altimetry tracks at low to middle latitudes and their low temporal frequencies (Baup et al., 2014).

2.5.2 Bathymetry

Many different data sources and techniques can be used to acquire elevation data and simulate the data into a continuous surface representing the real-world terrain. Traditionally elevation data was acquired through ground based surveying methods; however, with the increased acquisition of satellite RS data and improved techniques, elevation data can be retrieved more quickly and over larger spatial scales. DEMs can be obtained from contour lines, topographic maps, field surveys, photogrammetry techniques, radar interferometry, and laser altimetry.

As noted in Table 2.1, the availability of a DEM for SWS estimation is valuable as it allows the creation of empirical relationships to calculate storage. Tank systems pose a unique challenge in terms of retrieving accurate bathymetric information. The term bathymetry here refers to the topography beneath the water surface. For tank structures, accurate bathymetry (*i.e.*, detailed topographic profile) is difficult to retrieve for three primary reasons: 1) they are small and require detailed high-resolution information to capture their bathymetry; 2) they cover a large geographic extent; and 3) they are seasonally-filled water structures. Bathymetric information for tanks has been acquired during the dry-season when tanks are empty from traditional field topographic surveys (Van Meter et al., 2016) and more recently from unmanned surface vehicles (Young, Peschel, Penny, Thompson, & Srinivasan, 2017). The former bathymetric retrievals were only able to be captured because the tanks contained no water. Also, both former noted methods are limited by geographic scope and/or accessibility issues.

Extrapolated DEMs from different sources like Shuttle Radar Topography Mission (SRTM) or Advanced Spaceborne Thermal Emission and Reflection Radiometer (ASTER) DEMs have been used to approximate bathymetry (Peng, Guo, Liu, & Liu, 2006; Vaze, Teng, & Spencer, 2010; Venkatesan, Balamurugan, & Krishnaveni, 2011). Although the quality of the DEM (which

is a function of the spatial resolution and vertical accuracy of the data source) will influence the estimated SWS, it is unclear under what circumstances global DEMs are suitable for SWS estimation in small water bodies (Ouma, 2016). Currently, global SRTM and ASTER DEMs are available for S. India but are too coarse a spatial resolution to capture tank bathymetry (Appendix B).

Fortunately, the new TanDEM-X DEM, produced by DLR (German Aerospace Centre) is a new global DEM with unprecedented accuracy compared to the SRTM and ASTER datasets and is highly valuable for large-scale hydrological applications. The DEM has a spatial resolution of 10–12 m, and a reported height accuracy 2–4 m. This global high-precision DEM was developed using SAR interferometry (InSAR) from TanDEM-X and its twin satellite TerraSAR-X data flying in a close orbit formation to enable single-pass SAR interferometry. The final nominal 12 m spatial resolution DEM was then generated by stacking overlapping TerraSAR-X/ TanDEM-X radar pair DEMs. While the height accuracy of the 12 m resolution TanDEM-X product has been evaluated in various environments (Rizzoli et al., 2017), few studies in the literature have applied the novel data in hydrological applications (Zhang et al., 2016) and no study has evaluated the application of the TanDEM-X DEM for the retrieval of tank bathymetry.

2.5.3 Estimating lake/reservoir surface water (SW) extent

At different frequencies, water has distinct radiative properties that allow it to be distinguished from other land features. This unique response allows water to be detected from several passive and active satellite sensors (Huang, 2018). When weather conditions are favorable, optical sensors are the preferred information source due to their straightforward interpretability and abundant volume of data in terms of both temporal and spatial resolution (Gao et al., 2012; Huang, 2018; Liebe, Van De Giesen, & Andreini, 2005; Rodrigues & Liebe, 2013; Verpoorter,

Kutser, Seekell, & Tranvik, 2014). For example, the S2 sensor currently provides data every five days with a high spatial resolution of 10 m. Water is easily distinguished spectrally in the visible-infra-red region of the electromagnetic (EM) spectrum with characteristically low reflectances over visible wavelengths and lower or no reflectance in the near-infrared (NIR) and short-wave infrared (SWIR) wavelengths. Depending on water quality and sediment concentration, water reflectance is variably across the NIR and SWIR wavelengths and as shown, increased sediment concentration increases reflectance (Figure 2.5).

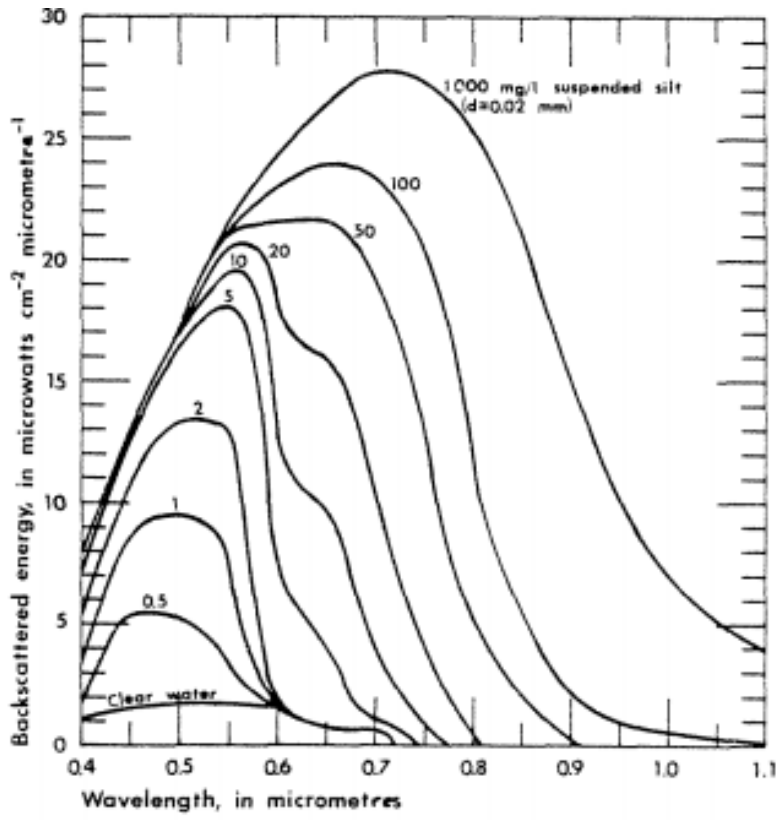

Figure 2.5: Reflectance versus wavelength (visible-SWIR) for water and increased sediment concentrations. (Retrieved from Moore, 1980)

Despite the merits of optical data for surface hydrology studies (*i.e.*, easy distinguishability and high accessibility) (Huang, 2018), a limitation of multispectral imagery is its dependence on

cloud-free acquisitions. This is a crucial disadvantage for monitoring waterbodies in semi-arid monsoon dominated climates because cloud cover prevails during the main precipitation events, which makes the application of optical RS data for operational monitoring inadequate. A detailed review of the applications for the detection, extraction, and monitoring of SW extent using optical satellite platforms can be found in Huang (2018) in which a compelling case is made for the use of radar observations for hydrology monitoring as a possible alternative for, or complement to, optical imagery (Huang, 2018). Unlike optical sensors, active microwave or radar (**RA**dio **D**etection **A**nd **R**anging) sensors (within the 3–10 GHz) range can potentially collect data from large areas under any weather conditions, allowing for continuous and repeatable observations.

2.6 SAR RS for the characterization of tanks

Inland water monitoring using SAR observations has been the object of study for many researchers for over two decades (Behnamian et al., 2017; Bioresita, Puissant, Stumpf, & Malet, 2018; Bolanos, Stiff, Brisco, & Pietroniro, 2016; Bonn & Dixon, 2005; Cazals, Rapinel, Frison, Bonis, & Mercier, 2016; Clement, 2018; Dasgupta, Dwivedi, Kushwaha, & Bhattacharya, 2010; Kasischke et al., 2003; Matgen, Schumann, Henry, Hoffmann, & Pfister, 2007; Tholey, Clandillon, & Fraipont, 1997; Twele et al., 2016; Zeng, Schmitt, Li, Zhu, & Li, 2017). SAR is a side-looking imaging radar system (airborne or spaceborne) that utilizes the flight path of the platform to mimic an extremely large aperture electronically, generating high-resolution RS imagery. Many SAR sensors currently are in operation (*e.g.*, European Sentinels and Canadian Radarsat-2) or are scheduled for launch in the next few years (see Appendix C). This diversity in sensors offers a wide range of possibilities in terms of spatial resolution, wavelengths, revisit periods and polarizations. In the past four years, greater attention has been drawn by S1-A and B satellites, which were launched in April 2014 and April 2016, respectively by European Space Agency

(ESA) in the framework of the European Union's Copernicus Program (Bioresita et al., 2018; Cazals et al., 2016; Clement, 2018; Martinis & Plank, 2018; Twele et al., 2016; Zeng et al., 2017). Both Sentinel-1 satellites carry a C-band SAR and the data is freely available with increased temporal and spatial resolution compared to previous sensors (*e.g.,* ENVISAT, ERS).

2.6.1 SAR: theoretical considerations

SAR systems transmit and receive an EM wave with a specific wavelength (λ) and frequency (*f*). Unlike optical sensors, SAR systems generate their own source of energy, and the sensor receives the energy that is backscattered back from the target surface. When the incoming wave interacts with the ground surface or target, part of the energy is absorbed by the target and part of the energy is reflected and scattered. The fundamental form for describing the waveform interaction with the target is given by the monostatic radar equation:

$$P_r = \frac{P_t G^2 \lambda^2 \sigma}{(4\pi)^3 R^4} \tag{2.2}$$

Eq. (2.2) describes the relationship between the power that the target receives from the incoming EM wave and the power re-radiated by the same target in the form of a scattered waves. P_r is the power detected by the receiver, P_t is the power transmitted, G is the antenna gain, and σ is the backscatter coefficient of the target. Eq. (2.2) represents the power returned from a theoretical, distinct target and not the scattering behavior of real world terrain. This is not the case for EO targets on Earth as most power responses are formed of multiple targets, making them distributed in nature. As water surfaces are distributed targets, it is standard to normalize σ by the radar illuminated area (A), Eq. (2.3), to provide the normalized radar cross-section (σ) and the radar backscatter coefficient, also called sigma nought (σ^0), which is a power term measured in decibels (dB):

$$\sigma^0 = \frac{\sigma}{A} \tag{2.3}$$

Combining Eq. (2.2) and Eq. (2.3) to solve for σ^0 yields:

$$\sigma^0 = \frac{\sigma}{A} = P_r \frac{(4\pi)^3 R^4}{AP_t G^2 \lambda^2} \tag{2.4}$$

In Eq. (2.2), variables other than σ are defined by the sensor system parameters. If the sensor system parameters do not change, solving for σ determines the influence of the target properties on backscattered power. However, solving Eq. (2.2) requires understanding of sensor properties, such as frequency, polarization and incident geometry and surface properties (surface roughness and dielectric constant).

Different microwave frequencies (*f*) are used to transmit the EM energy in a SAR system, where *f* ranges from about 0.3 to 300 GHz (1 m–1 mm in λ). EO radars commonly have *f* below 20 GHz (Ulaby & Long, 2014) and operate at one explicit frequency within a narrow frequency band, which is an important characteristic of a radar sensor. These different frequencies (inversely proportional to wavelength) are often called bands and image the Earth's surface properties in different ways, depending on the frequency (wavelength) with lower (longer) frequencies (wavelengths) providing increased penetration though Earth surface materials than higher (shorter) frequencies (wavelength) (Figure 2.6). With respect to open liquid water, the ability of detection using radar is typically independent of frequency; microwave energy is highly sensitive to liquid water because its dielectric constant is highly reflective of the propagated wave (Ulaby & Long, 2014). The Sentinels operate in C-band (at 5.6 cm wavelength) and have been used for open water mapping (Brisco, Short, Van Der Sanden, Landry, & Raymond, 2009; Cazals et al., 2016; Martinis & Plank, 2018; Ottinger, Clauss, & Kuenzer, 2017); however other wavelengths such as X, and L band are also often used.

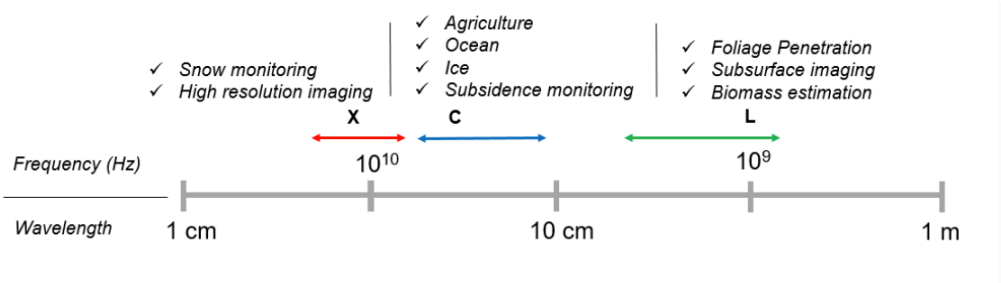

Figure 2.6: Schematic showing various application within the X, C and L-band frequency and wavelength regions of the EM spectrum.

Polarization refers to the orientation of the electric field of the propagated and received EM wave along its propagation axis as it travels from the transmitter to the target on the ground and back. When the transmitted or received wave is measured in the horizontal direction, the wave measured is the horizontally (H) polarized wave; conversely, when the wave is measured in the vertical (V) polarization state, perpendicular to the horizontal state, the wave measured is the vertically polarized wave (Figure 2.7). Relative to the Earth's surface, SAR systems primarily transmit and receive backscatter power in the horizontal or the vertical polarization state leading to four polarization configuration measurements: HH, HV, VV and VH. VV and HH polarization are defined as like polarized, and VH and HV are defined as cross-polarized. Although each polarization state can be used for water delineation, the backscatter characteristics of the radar signal can vary depending on water quality, surface roughness and incidence angle, impacting the accuracy of the water maps produced (Annor et al., 2009; Bolanos et al., 2016; Brisco, Kapfer, Hirose, Tedford, & Liu, 2011; Liebe, Giesen, et al., 2009; Manjusree, Kumar, Bhatt, & Rao, 2012).

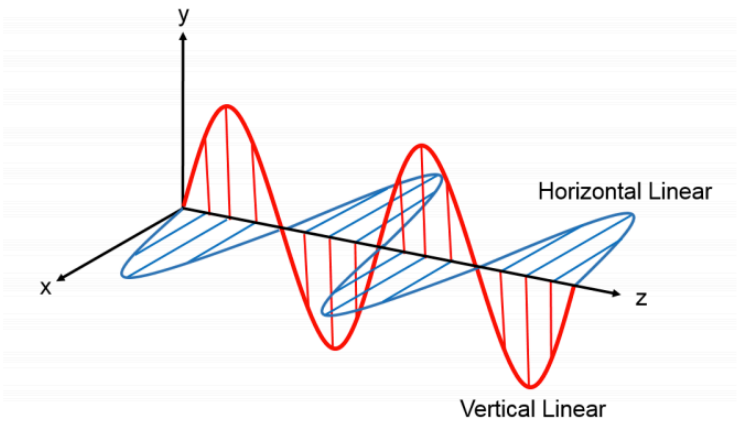

Figure 2.7: Example of linearly polarized wave, showing horizontal polarized wave and vertically polarized wave.

For the S1 SARs, the interferometric wide swath (IW) is the default imaging mode covering land surfaces and observations are acquired in a dual-polarized manner with VV and vertical VH state measurements. Most studies have shown that HH polarization is better suited for water mapping (Bolanos et al., 2016; Brisco et al., 2011, 2009; Manjusree et al., 2012); however, some studies showed that good results can be obtained with HV (Henry, Chastanet, Fellah, & Desnos, 2006) polarization and VV (Martinis & Plank, 2018) polarization. Since reflections of smooth open water are primarily like-polarized, VV is better suited for extracting SW area (Liebe, Giesen, et al., 2009; Martinis & Plank, 2018). However, VV polarization is also more sensitive to wind-induced roughness over open SW compared to HV (Behnamian et al., 2017; Brisco et al., 2011; Henry et al., 2006). Using the same polarization different water bodies on the same date can present large variations in backscatter. Figure 2.8 presents a result from Manjusree et al. (2012) who examined SAR signature ranges for C-band data for varying water bodies, one of which was tanks in Northern India (Manjusree et al., 2012). Unlike flood water, backscatter for other water bodies, including tank water, is typically low due to calmer SW and low roughness states.

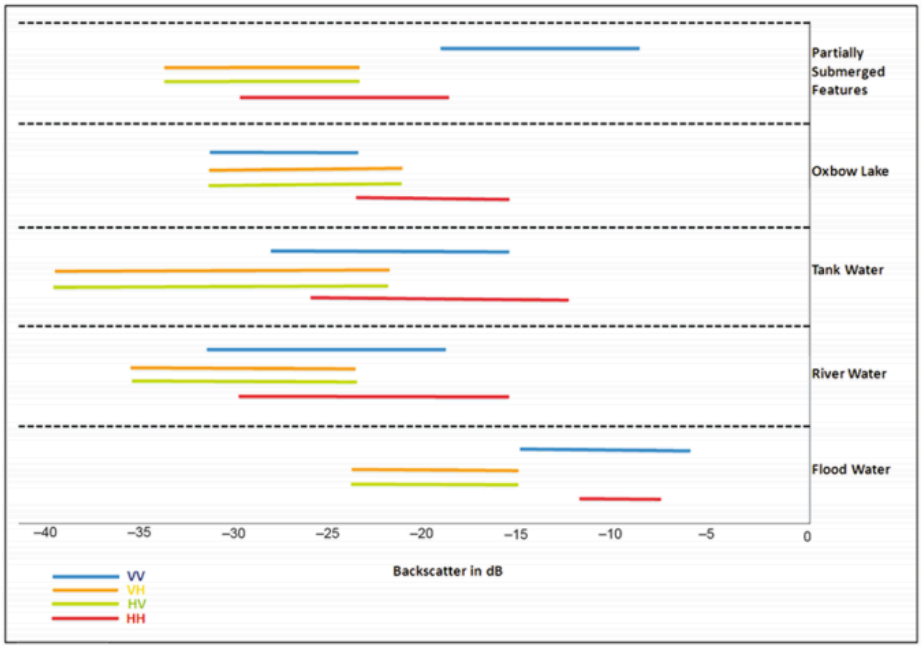

Figure 2.8: Result from Manjusree et al. (2012) that shows variation in backscatter among five different SW regions for four polarizations.

In addition to the former noted system specific properties, the objects specific (surface roughness and dielectric constant) influence the radar backscatter. Focusing on smooth open water, water acts as a specular reflector causing most of incident energy away from the sensor (Figure 2.9). Thus, open smooth water surfaces appear dark in SAR scenes because of very low signal return. Also, due to the high dielectric constant of water (about 70 at C-band), the penetration depth of the radar signal into the water is low (Eilander, Annor, Iannini, & van de Giesen, 2014). This results in low volume scattering and depolarization and therefore mostly like-polarized reflection. For this reason, when water is calm, backscatter in like-polarized bands tends to be higher than cross-polarized bands.

However, water bodies are often not smooth and instead the surface roughness of water bodies is highly variable (Figure 2.9). For this reason, even the same water bodies overtime present large variations in backscatter. Furthermore, vegetation at the tail ends of the reservoir during the

dry-season and lack of backscatter from surrounding dry areas causes further problems when extracted SW from a SAR scene (Annor et al., 2009; Eilander et al., 2014). Both wind and rain are known to increase surface roughness and in turn increase backscatter (Eilander et al., 2014). This causes the land and water contrast to diminish, making it difficult to accurately extract SW.

In addition to surface roughness influencing radar backscatter, the backscatter also varies as a function of incidence angle. As shown by Figure 2.10, for smooth surfaces, such as calm water, when the incidence angle is small, the water surface acts like a mirror. As incidence angle increases, the radar backscatter intensity continuously declines and the rate of this decline is also variable for different surfaces.

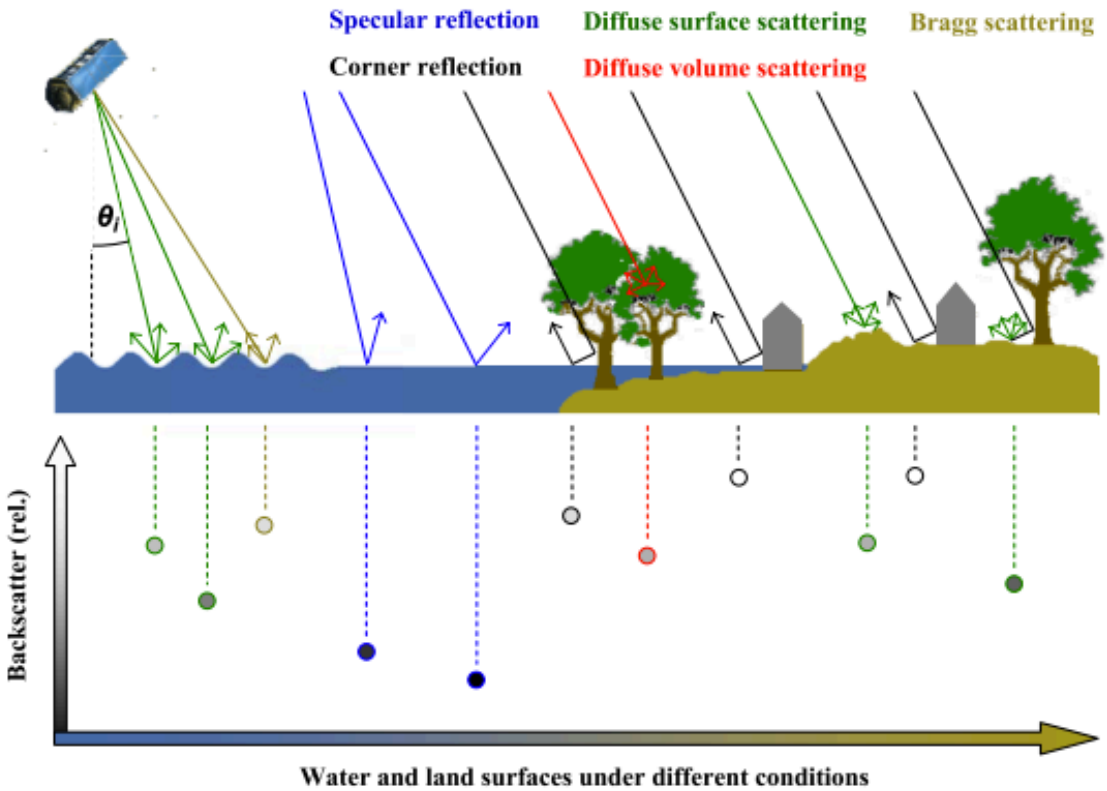

Figure 2.9: Scattering mechanisms of water and land surfaces as a result of changes in incidence angle and surface roughness (retrieved from Martinis, 2010)

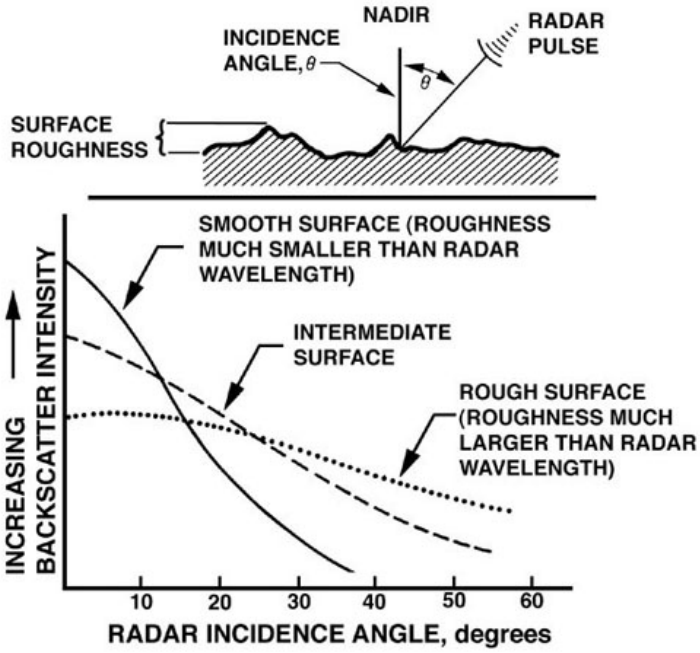

Figure 2.10: Relationship between incidence angle and radar backscatter for three surfaces. Retrieved from (Mark, 2018)

2.6.2 Water extraction

For the extraction of SW area from radar, many methods have been implemented with various levels of automation. The most commonly used approach to delineate water-land boundaries, also used herein, is a grey-level threshold-based procedure (Bolanos et al., 2016; Clement, 2018; Martinis & Plank, 2018; Twele et al., 2016). For grey level intensity thresholding, all pixels in the SAR image are mapped as water when their backscatter coefficient is lower than a specific threshold based on intensity ranges sampled in regions of known water (Behnamian et al., 2017). The backscatter distribution over a water body can be variable between SAR acquisitions and is largely influenced by weather (surface roughness), polarization, and incidence angle. For this reason, thresholds need to be determined uniquely per scene (Bolanos et al., 2016). Beyond a global threshold, where the threshold remains constant for the entire scene, it is also

common to set local thresholds, where a scene is subdivided and has threshold value chosen for each region with the scene. Although grey-level threshold-based procedures are easy to implement, determining a threshold is difficult and the technique of threshold selection is largely dependent on the required level of automation for SW extraction.

2.7 Sentinel-1 system and Google Earth Engine (GEE) considerations

Harmonizing the large amounts of open-access EO observations is increasingly possible using enhanced modern information and communication technology such as hosted computing platforms and services (*e.g.* cloud computing). Beyond data storage limitations, often RS applications face the challenge of limited computational capabilities. While cloud computing technology combined with RS analysis is still in its infancy, its use is growing rapidly. Efficient monitoring applications of wide area Earth systems can benefit from cloud computing. This is especially the case for tank monitoring systems which cover wide areas and need frequent high spatial resolution observations. Tanks structures are continuously changing and long term continuous monitoring of tanks during the monsoon seasons is critical. While several cloud-computing platforms exist for RS processing, a well-known example is the Google Earth Engine (GEE). GEE provides the possibility to develop algorithms in an environment which is directly linked to mass EO data collections (*e.g.* from Landsat, S1, S2). For the SW detection of tanks noted in Chapter 3, all S1-A, L8, and S2 data were retrieved directly from the GEE data catalog. The GEE S1-A and B collection includes Ground Range Detected (GRD) scenes, processed using the S1-A Toolbox to generate calibrated, ortho-corrected products. Pre-processing steps before ingestion to GEE included: updated orbit metadata, thermal noise removal, radiometric calibration and terrain correction (orthorectification).

2.8 Uncertainties in the RS DEM product

As noted previously, the TANDEM-X DEM dataset provides high spatial topographic information and has the potential to be applied for tank bathymetric retrieval. Despite its promising spatial resolution, a known limiting factor of the TanDEM-X DEM product is the time of acquisition ranging over multiple years and for tank bathymetry this is of critical importance. Tanks are seasonal storage structures and some tanks have been dry for many consecutive years. This thesis will not focus on the detailed information about the InSAR technique (for more information see Rossi et al. (2012) (Rossi, Gonzalez, Fritz, Yague-martinez, & Eineder, 2012). However, an important point to note is that high coherence between satellite overpasses is a requirement of accurate DEM generation using InSAR. The final TanDEM-X-DEM is comprised of the combination of data sets acquired at different dates with time spans up to a year and as a result, the appearance of water bodies can vary. In the case of tank structures, variability between scenes and in turn a reduction in coherence is introduced due to seasonally changing water levels. Fortunately, along with their TanDEM-X DEM product, DLR provides a Water Indication Mask (WIM) to support the TanDEM-X-DEM editing process (Wendleder et al., 2013). The WIM provides a value representing the frequency, where the higher the frequency of classification, the more reliable the pixel represents water. While the highest frequencies (*i.e.*, water presence located in every single interferometric data set) and lowest frequencies values (*i.e.*, no water presence located in any single interferometric data set) of WIM in conjunction with the TanDEM-X DEM are easy to determine the reliability and usability of the associated TanDEM-X elevations, the middle frequencies (*i.e.*, water presence located in some single interferometric data sets) is not clear. In these cases, in situ data should be used in combination with the WIM mask to determine

its suitability and accuracy for the retrieval of bathymetry in water bodies using the TanDEM-X DEM product.

The above concern lead the rationale to collect a detailed topographic field survey of four tanks within the upper Gundar basin (Figure 2.1b). The field survey was carried out over four tanks in the Gundar basin using a Trimble S6 Robotic Vision Total Station together with a 360 degree Multi Track prism (Appendix A). The survey was completed from 20th June-13th July with a total of approximately 2,791 points collected and an area of 126 ha covered by the survey. The conventional field survey was conducted like a standard topographic survey but the focus was only upon mapping the shape and elevation variations of the terrain accurately. A cross section or point spacing of approximately five m was adopted except where terrain variation required denser data. Vigilance was utilized to ensure the data was accurate. Pole heights were regularly checked by measuring a known mark before starting survey work. Instrument and backsight targets were measured accurately and checked. Stations were located to permit maximum inter-visibility to other marks and measurements were taken where extra control marks could be seen. The field surveys were completed a few days ahead of schedule which allowed all four tanks to be revisited to QA/QC results. This consisted of traversing the tanks while observing the generated DEM at each location and noting significant anomalies. The topographic surveys as well as the visual inspection of several tank structures observed from the TanDEM-X DEM supported the application of the DEM to approximate tank bathymetry. Based on these validation measures, the assumption was made that the TanDEM-X DEM elevations reach close to the tank bed and as such, the dataset was used to obtain volumetric estimates.

2.9 Rationale for manuscript

The previous sections provide the background to the following study of tank monitoring in S. India which serves several purposes. From an application perspective, there is currently no RS-based method to estimate tank SWS. Unlike other inland water bodies, tanks are particularly challenging to monitor due to their small geographic size and limited *in situ* data to support RS-based estimates. The manuscript serves primarily to highlight a potential methodological approach for SWS storage in tanks and the application examples are provided only to give context to the potential application of the tank SWS estimation approach. From a methods perspective, an effort was made to utilize GEE JavaScript application program interface (API) for RS data preprocessing and analysis. By using GEE for data access and analyses, there is a potential to extend this analysis to other local and/or regional scales.

Given the current limited water availability from groundwater reserves and interannual variability in monsoon events in S. India, the amount of water in tanks should be quantified to improve or at least be considered in local resource water planning. At present, the magnitude and variability of water in tanks can be inferred from SW extent from several satellite and aerial observations but the value of these observations would increase dramatically if water extent observations could be related to SWS (*i.e.*, water volume). For tanks, remotely sensed surface elevation estimates from radar altimeters are too coarse in spatial resolution for water level retrievals. Therefore, a DEM in addition to satellite extracted SW observations is the only current means to estimate SWS during monsoon periods. Fortunately, the novel DEM data set from TanDEM-X provides an opportunity, for the first time, to retrieve tank bathymetry at large spatial scales. Therefore, the paper that comprises Chapter 3 is entitled “Estimating seasonal surface water storage in rainwater harvesting reservoirs in southeast India using satellite remote sensing”, and

utilizes a novel high-resolution DEM, that (for the first time) captures the bathymetry of tanks at a large spatial scale. The research aims to evaluate whether tank volume estimates derived from the combination of empirically generated power-like models and SW estimates are a) appropriate and b) can be used to monitor tank volumes given the extensive amount of available EO data.

Chapter 3

Estimating seasonal surface water storage in rainwater harvesting reservoirs in southeast India using satellite remote sensing

3.1 Summary

India's vulnerability to water shortage and scarcity demands a critical understanding of the hydrological role of rainwater harvesting tanks (reservoirs) at multiple spatial scales. This study describes a remote sensing (RS) approach to water volume monitoring in small reservoirs (5-80 ha) in the Gundar Basin, Tamil Nadu state in S. India. Empirically-derived water storage relationships were evaluated using TanDEM-X digital elevation model (DEM) data combined with estimates of the surface water (SW) area from C-band Sentinel-1A (S1-A) synthetic aperture radar observations, Landsat-8, Sentinel-2, and PlanetScope visible/infra-red observations. The TanDEM-X DEM data revealed strong power-type relationships between surface area and storage volume, and were combined with satellite SW observations to estimate and monitor tank volumes. Three models of volume-area (V–A) relationship(s) were assessed: the tank specific (TS) model, a size-dependent categorical (CAT) model and a generalized (GEN) model for all tanks. For volume estimation, the CAT model produced the lowest root mean squared error (RMSE) as a percentage, V_{ERR}, of volume for the basin. While tank SW area was estimated using S-1A data, the narrow SW area of some tanks, especially close to the retaining wall presented challenges for operational use. Two examples demonstrate the approach: 1) the maximum volume of water in

559 tanks in the basin for two monsoon seasons and 2) a time-series analysis using a high-volume of satellite observations shows the cycle of water (inflow and outflow) at the tank scale. This study illustrates the applicability of using a satellite RS observation approach to continuously monitor rainwater harvesting, and beyond this, the critical need of an adopted multi-sensor (optical and radar) monitoring approach.

3.1 Introduction

Reservoirs are essential for the development and management of water resources in a river basin (Liebe, Van De Giesen, & Andreini, 2005). In S. India, thousands of traditional small storage reservoirs, termed 'tanks', are used as rainwater harvesting (RWH) systems to harvest, store and supply rainwater for domestic and agricultural use (Van Meter et al., 2016). With a growing awareness in water security, these traditional structures built decades ago are now being re-examined as a way of increasing water storage and supply (Aubriot & Prabhakar, 2011; Kumar et al., 2008; Shah, 2004), yet there is a gap in knowledge on their distribution and storage capacities. With the large-scale interest in the restoration of these systems, it is critical to have a method of monitoring tank water volume variations and with approximately 120,000 tanks in S. India alone (Gunnell & Krishnamurthy, 2003), capturing these variations on a regular basis is not feasible from conventional field-based measurements. RS techniques and Earth observation (EO) data are promising tools to overcome the difficulty in estimating reservoir volume state, at a minimal cost, and also provide the potential to systematically monitor the vast number of tanks present in the landscape. With this information, hydrological research can begin to quantify the hydrological water balance at tank, cascade and basin scales (Bitterman et al., 2016).

RS methods have been used to characterize and monitor a range of continental inland water bodies (Baup et al., 2014; Frappart, Seyler, Martinez, León, & Cazenave, 2005; Medina, Gomez-

Enri, Alonso, & Villares, 2010; Musa, Popescu, & Mynett, 2015). For reservoir storage estimation using satellite RS, the common approach is to retrieve elevation and surface water (SW) area separately, and then combine these two variables for calculating the storage (Crétaux et al., 2011; Gao et al., 2012). For elevation, satellite radar and laser altimetry are the common approaches to estimating the elevation of open water bodies, their water level or bathymetry (Crétaux et al., 2011; Frappart et al., 2005). For SW area, studies have successfully delineated the water extent with optical sensors or radar images (Gao et al., 2012; McFeeters, 1996; Musa et al., 2015). In S. India, remotely sensed surface elevation estimates from radar altimeters are too coarse in spatial resolution for water level retrievals of small tanks less than 80 ha in size (Baup et al., 2014). An alternative approach, based on empirically-derived storage relationship(s) combined with estimates of the SW area from RS satellite observations, can be followed for tank monitoring (Annor et al., 2009; Liebe, Van De Giesen, Andreini, Walter, & Steenhuis, 2009; Magome et al., 2003; Minke & Westbrook, 2010; Sawunyama et al., 2006).

The success of water resource management depends on the accurate assessment of water availability in tanks at the watershed scale. Therefore, the objective of this study is to provide a RS-based tank volume monitoring approach, which can be used for water resource management and Earth system modeling applications. This RS-based method consists of deriving empirical storage relationship(s) using a high-resolution global digital elevation model (DEM) and satellite synthetic aperture radar (SAR) observations for the retrieval of SW area. The study seeks to (i) evaluate the utility of volume-area (V–A) relationship(s) for small reservoirs located in the Gundar river basin and (ii) demonstrate time-series volume estimation by combining V–A relationship(s) and SAR and optical satellite observations.

3.2 Datasets and study area

The data sources and their purposes are listed in Table 3.1. Processing and analysis of SAR and optical data sources were performed in the Google Earth Engine (GEE) cloud computing platform with a Java API interface (Gorelick et al., 2017).

Table 3.1: Satellite and field data sources for the validation and estimation of water surface area in tank systems (Purpose: 1= Calibrate V-A method, 2 = Monitoring application).

Data	No. of images	Date	Provider	Purpose
Field GPS Elevation	n/a	July 2016	Topographic field survey with total station	1 (§3.3.5)
Sentinel 1A (S1-A)	44	Sept.–Dec.2015, 2017	Google Earth Engine's public data catalog	2 (§3.3.7)
	5	Sept.–Oct. 2017		1 (§3.3.6)
Planet Scope (PS)	20	Sept.–Oct. 2017	Planet through the Education and Research Program	1 (§3.3.6)
	27	Aug. 2017–Jan. 2018		2 (§3.3.7)
TanDEM-X DEM	2	n/a	DLR through proposal titled *DEM_HYDR0751*	1 (§3.3.2)
Landsat-8 (L8)	3	2017-08-23, 2017-10-10, 2017-12-29	Google Earth Engine's public data catalog	2 (§3.3.7)
Sentinel-2 (S2)	4	2017-08-22, 2017-09-06, 2017-10-01, 2017-10-21	Google Earth Engine's public data catalog	2 (§3.3.7)

3.2.1 Satellite C-band SAR observations

20 m pixel spacing SAR Sentinel-1 (S1-A) observations were selected for this study. S1, part of the European Space Agency Copernicus programme, is a constellation of two polar-orbiting C-band SAR satellites. The 2015 and 2017 years were selected for water monitoring because tanks received significant precipitation. A total of 49 S1A dual-polarization (VH+VV) Interferometric Wide Swath mode products were used, delivered in Ground Range Detected High Resolution mode. Radiometrically calibrated and terrain corrected S1 images are stored in GEE, meaning that each scene was pre-processed with the S1 Toolbox in GEE using the following steps: 1) thermal noise removal; 2) radiometric calibration; and 3) terrain correction using SRTM 30. Additionally,

in GEE, a median filter with a 4 × 4 window was applied to reduce speckle noise within each scene.

3.2.2 Satellite visible/infra-red observations

3 m PlanetScope (PS) data (Planet Team, 2017) were acquired for this study. PS imagery has four bands, blue (Band 1, 455–515 nm), green (Band 2, 500–590 nm), red (Band 3, 590–670 nm) and near infrared (Band 4, 780–860 nm). For the validation of the SW area, 20 PS Level 3A data product scene swaths (~ 225 km^2 each) were acquired for the listed 2017 dates: Sept. 2 (n = 8), Oct. 1 (n = 6), and Oct. 8 (n = 6). These specific images were chosen because they match a S1-A acquisition date and had minimal cloud cover. An additional 27 cloud-free PS images were acquired between August 2017–January 2018 to extract a time-series of SW area. All PS were calibrated to top of atmosphere reflectance and imported to GEE. Three 30 m L8 and four 10 m S2 images were also used. L8 imagery has 11 bands, but only the green (Band 3, 533–590 nm) and near infrared (Band 5, 85-0.88nm) bands were used. The green band was used instead of SWIR bands due to high sediment content in tank water (Appendix A). Similarly, from the 13 S2 bands only the green (Band 3, 0.560 nm) and near infrared (Band 8, 0.842 nm) bands were used.

3.2.3 TanDEM-X DEM product data

This research relies on a DEM to estimate the topography/bathymetry of selected tanks in the basin. The highest spatial resolution global DEM available was obtained. The TanDEM-X DEM, produced by DLR (German Aerospace Centre) from a five year (2010–2015) radar satellite mission and interferometric techniques, provides a DEM with a spatial resolution of 10–12 m, and a relative height accuracy of 2–4 m (Eineder, Adam, Bamler, Yague-Martinez, & Breit, 2009). To cover the entirety of the basin, two tiles were mosaicked and imported into GEE. Early

investigation revealed that other global DEM products were insufficient to capture the small-scale topography of the tanks, making the TanDEM-X DEM critical for this work.

3.2.4 Gundar River Basin and reservoir selection

A river basin with a large concentration of tanks was selected for detailed study; the Gundar River Basin (5647 km^2) in the S. Indian state of Tamil Nadu (Figure 3.1). The region is dominated by tropical monsoon climate seasons, receiving a mean annual rainfall of 770 mm from three distinct periods: the Southwest monsoon from June–September (25 % of annual rainfall), the Northeast (NE) monsoon from October–December (50 % of annual rainfall), and the dry season from January–May (25 % of annual rainfall). Tank structures have been constructed across natural depressions in the landscape to capture surface runoff and rainfall. Water is impounded behind an earthen embankment (a bund) and is released through sluices into canals to be further distributed to irrigated lands. Irrigation tanks are linked in cascades, with overflow channels providing connections to tanks downstream. These connected systems form a complex hydrologic network of man-made wetlands across the landscape, ranging in size from 20×10^5 m^2 to 80×10^5 m^2 (Van Meter et al., 2016).

A hand-digitized shapefile of tank locations was used to gain an understanding of their distribution. Of the 5647 km^2 total study area, 2314 tanks cover 9 % of the land surface. Given the spatial heterogeneity in tank size, the cumulative distribution of tanks is not linear (Figure 3.2, Table 3.2). Table 3.2 shows that large tanks (> 100 ha) contain 24 % of the total tank water storage area despite representing only 3 % of the total number of reservoirs. In contrast, smaller tanks (10-100 ha) occur at the highest frequency and represent 67% of the total water storage area. Despite the large concentration of tanks, only 1503 tanks have received water in the last 25 years as observed from Landsat satellite observations (Pekel et al., 2016). For this work, the focus was on

tanks within the sample of 1503 that are also between the size range of 5-80 ha. This results in 559 tanks (103 km^2) for water volume monitoring over two monsoon seasons.

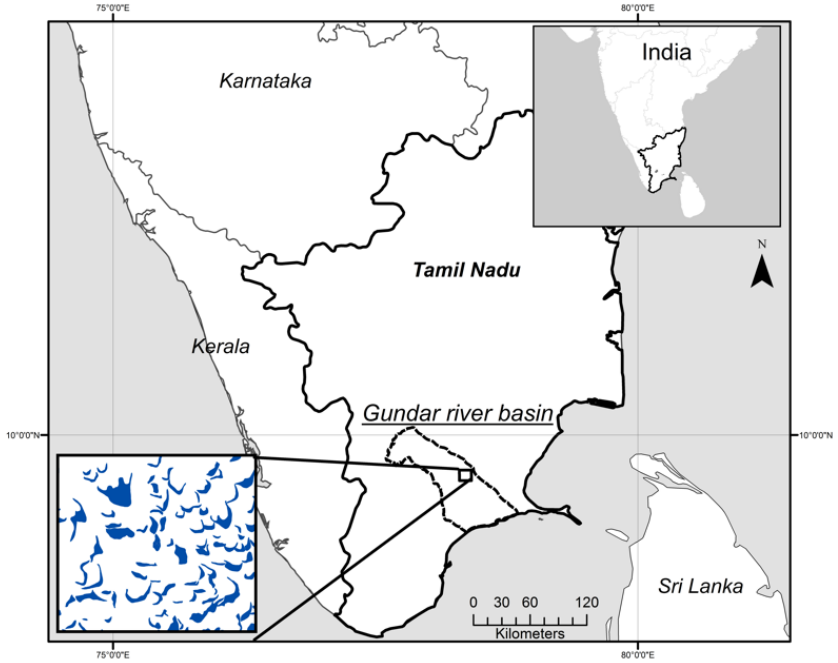

Figure 3.1: The location of the study area – the Gundar River Basin in Tamil Nadu, India. The left inset shows tanks across the landscape

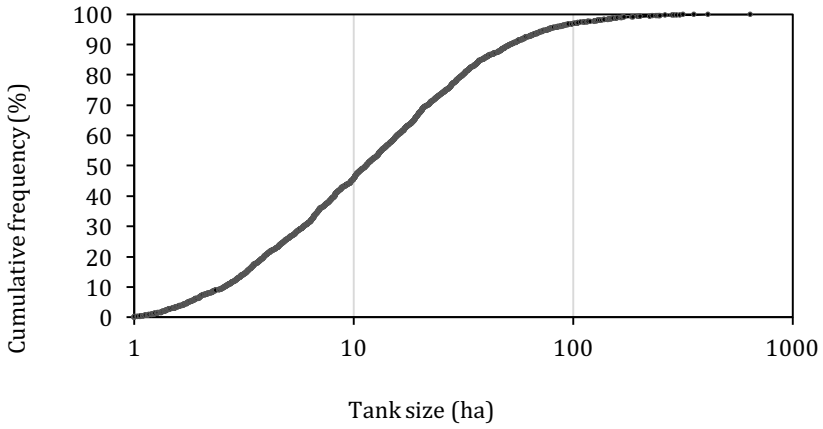

Figure 3.2: Cumulative distribution of tank size (n=2314)

Table 3.2: Number of tanks in basin categorized by size and their SW area

Tank Size, ha	Number of Tanks	Total Surface Area, km^2	Relative Water Surface Area, %
1-10	1051	50	9
11-100	1191	350	67
>100	72	126	24
Total	2314	526	100

3.3 Methods

3.3.1 Surface water estimation

SW retrieval using SAR data has been the subject of several studies (Bolanos et al., 2016; Brisco et al., 2009; Medina et al., 2010). SAR data is particularly suited to SW monitoring in persistent cloud-covered monsoon environments because of its all-weather capability and moderate-high spatial resolution. For operational SW estimation, image histogram threshold-based procedures are widely implemented because of their simplicity. The key parameter in the thresholding process is the automatic choice of the threshold value. The Otsu (1979) method was selected due to its tractable implementation in the GEE environment. The method partitions a histogram into *n* classes by iterating through all possible histogram threshold values (per scene). The final threshold is specified as the value at which the sum of the variances for the sub-modal distributions (water and land classes) is minimized (Figure 3.3).

For SW retrievals from the SAR data, a tank mask buffer of 200 m surrounding each tank was generated. SAR scenes were clipped to the mask and the Otsu algorithm was run to generate a unique threshold (VV and VH polarization) per masked SAR scene. This local threshold was selected on a tank by tank basis per satellite scene to reduce the effect of the incidence angle in the threshold selection process. Masked pixels below the Otsu-defined threshold were labelled as water and above the threshold labelled as land. Each image was converted to vector format and

subsequently, the SW area for each vector was calculated.

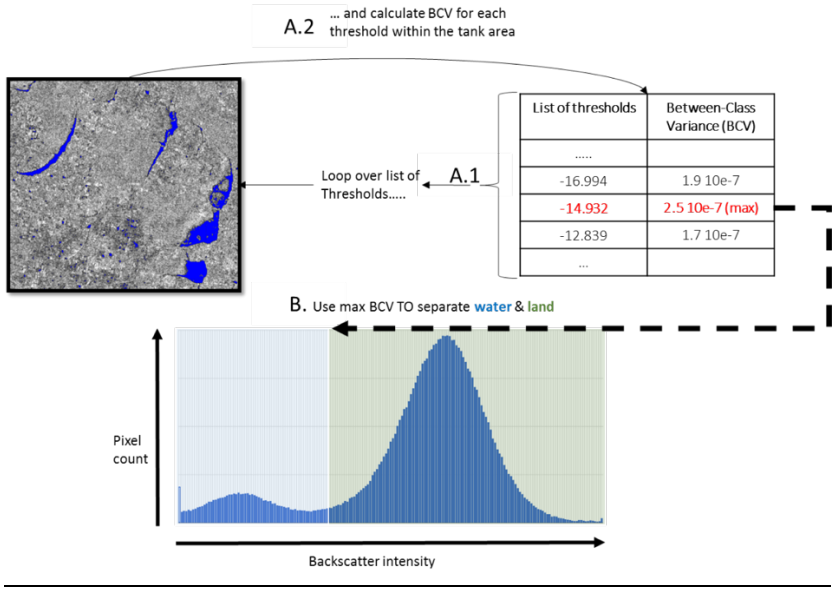

Figure 3.3: Concept of the implemented Otsu method to separate water from land in tanks. A.1 and A.2 define a loop, resulting in finding the threshold which corresponds to the maximum Between-Class Variance shown in B.

3.3.2 Derivation of reservoir Volume–Area (V-A) relationships

The theoretical basis to estimate total reservoir water storage is developed on the assumption that a reservoir shape can be simplified as a square pyramid diagonally cut in half (Magome et al., 2003). Tank water volume (V) can be estimated from reservoir SW area (A) using an empirical relationship (Magome et al., 2003). Power law expressions have been demonstrated as effective storage-discharge model predictors for the hydrologic modelling of small reservoirs (Young et al., 2017):

$$V = aA^b \tag{3.1}$$

where V is the volume of the reservoir (m^3), A is its SW area (m^2), a is a scaling coefficient and b is an exponent indicating the rate of growth or decay. For the generalized case of a half pyramid geometry reservoirs, $b = 1.5$, while $b > 1.5$ if the slopes are more convex and $b < 1.5$ if slopes are more concave. While the power model is robust for idealized hydrologic modelling (Annor et al., 2009; Liebe, Van De Giesen, Andreini, Walter, & Steenhuis, 2009), the a and b parameters vary with natural geomorphic heterogeneity (Liebe, Van De Giesen, & Andreini, 2005; Meigh, 1995; Sawunyama, Senzanje, & Mhizha, 2006); over smaller distance scales the parameters a and b might be expected to remain constant (Annor et al., 2009) while over larger scales they might vary. Therefore, the challenge lies in finding the a and b parameters that minimize the error in the volume estimates.

To derive a V-A relationship of any given tank, TanDEM-X DEM data were used to provide paired volume and area estimates for the tank at 5 cm height increments from the base of the tank to the bund (*i.e*. the top of the dam, h_{max}) (see Appendix D). Using this method, a sample of 72 from the 559 (13%) small reservoirs were selected to generate V-A relationships for the reservoirs in the basin. The 72 tanks were selected by clustering the 559 tanks into four size groups and taking a proportional sample of suitable tanks from each group (Table 3.3). For each of the tanks, TanDEM-X DEM data and high resolution imagery were used to visually inspect for minimal water and vegetation presence to ensure that the bathymetry of the tank was accurately represented. In addition, for each size class only tanks with a bund height of at least 3 m (typical bund height) were selected.

Table 3.3: Proportional sample from each tank size group.

Size Class	Count	Proportion	Sample Count
<10	183	0.33	24
10-20	183	0.33	24
20-50	135	0.24	17
>50	58	0.10	7
Total	*559*	*1.00*	*72*

Having selected the 72 samples, three models were parameterized to explore scalability of the *a* and *b* coefficients needed for Eq. 3.1: the tank specific (TS) model, categorical (CAT) model and the generalized (GEN) model. For the TS model, Eq. 3.1 was fitted using linear least squares regression to each tank in the data set (n=72). Hence, there were 72 unique *a* and *b* coefficient pairs. Analysis of the TS model was included to identify the *a* and *b* coefficients that best describe each tank's morphometry, assess the overall suitability of power functions to describe tank bathymetry, and estimate the water volume using TS metrics. The CAT model sought to fit a generalized model for each size category in Table 3.3. *a* and *b* coefficients were fitted to generate four unique equations with category-specific *a* and *b* coefficients. Analysis of the CAT model provided an opportunity to assess the accuracy of generalized equations relative to the TS model. Finally, the GEN model provided single *a* and *b* coefficients that were fitted to all tanks, regardless of size. This was the most generalized model. Analysis of the GEN model provided an opportunity to compare volume estimates for the TS and CAT models.

3.3.3 Added metrics for volume estimation

A tank's water storage capacity is defined by its bathymetry, and can be directly calculated if an accurate topographic survey is available. However, if the height accuracy and/or spatial resolution of the DEM is low, other metrics can be invoked to explain V_{max}. Maximum surface area (A_{max}) (m^2) of the tank at the maximum water height (H_{max}) was used along with the length of the

bund (B_{len}) and a dimensionless shape index (S_I) to describe the shape of the tanks water surface. S_I is the ratio of the tank perimeter to the circumference of a circle with the same area (Eq. 3.2):

$$S_I = \frac{P}{2\sqrt{\pi A_{max}}} \tag{3.2}$$

where P is the perimeter of the tank (m). Tanks with $S_I = 1$ have shapes that are perfectly circular, whereas tanks with $S_I > 1$ are increasingly complex. Tank shape is an important metric because the V-A relationship is predicated on the half-cut four-sided pyramid standard bathymetry. Therefore, using the S_I metric provides an opportunity to characterize any variance from this standard (Karran, Westbrook, Wheaton, Johnston, & Bedard-haughn, 2017; Minke & Westbrook, 2010). Regression and correlation analysis was performed to determine if any significant relationships exist between the morphometric variables, a, b and V_{max}.

3.3.4 Error Assessment: V–A model assessment

The root mean squared error (RMSE) of the volume estimate for each tank was calculated between the predicted volume from each model (TS, CAT, GEN) and the "reference" volume from the DEM. V-A estimates were compared with reference volume estimates at 0.05 m fill increments from empty to 100 % of h_{max}. A standardized error, V_{ERR} (%) for volume, was calculated by dividing the RMSE by V_{max}. This enabled comparisons of error between the different tanks and models regardless of tank size. In addition, V_{ERR} was calculated for two additional fill cases: 80 % of h_{max} and 50% of h_{max}. These additional depths were selected to test inconsistencies in error magnitudes when the tanks do not fill completely (Minke & Westbrook, 2010). Figure 3.4 shows that the largest volumetric differences typically occurs at stage levels above 1.5 m and the spillover

elevation in each tank (located at the top of the bund at ~ 3 m). Studies indicate that tank water levels rarely reach spillover elevation (Young et al., 2017) and in Tamil Nadu average tank water depths rarely exceed 1.5 m (Vaidyanathan, 2001).

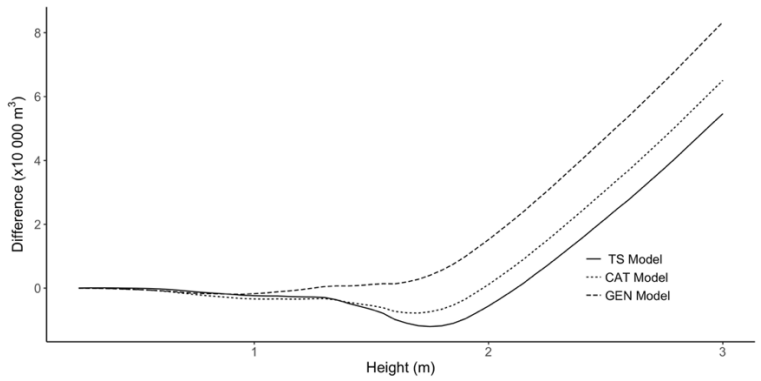

Figure 3.4: Difference in volume from "actual" volumes compared to predicted volumes from TS, CAT and GEN models for a selected representative tank.

3.3.5 TanDEM-X DEM

The accuracy of the TanDEM-X DEM product was evaluated using a topographic field survey of four tanks conducted in 2016, with a total of 2300 traditional survey points. The absolute elevations were compared, and V-A power relationships were derived and compared for each of the four tanks based on both field survey and TanDEM-X DEM data.

3.3.6 SW Area estimation

S1-A water classifications were validated by comparing them to tank water boundaries delineated from 3 m optical PS data acquired on the same date. Since, the PS data is not available for the basin until May of 2016, SAR data for 2017 were used for the SW validation. Three additional S1-A scenes were acquired from 2017 with 34 tanks from the Sept 2. image, 26 tanks from the Oct 1. image and 51 tanks from the Oct. 8 image. SAR SW area estimates were derived

using the Otsu algorithm (see §3.3.1). For SW extraction from PS, a Normalized Difference Water Index (NDWI) was calculated for each image:

$$NDWI = \frac{(\rho_{545} - \rho_{830})}{(\rho_{545} + \rho_{830})} \quad (3.3)$$

where ρ_{545} and ρ_{830} are the band reflectances at 545 nm and 830 nm respectively. Analysis of the NDWI PS scenes revealed that selecting arbitrary threshold reflectance values per scene to distinguish water from non-water surfaces was highly variable between scenes. Therefore, a 100 m buffer was generated for each tank polygon, yielding a buffered polygon mask containing both the maximum extent of water and some surrounding land and vegetation. The buffered tank polygons were intersected with the NDWI for each image and Otsu thresholding was used to delineate SW in each image. The SW area in each image were then converted to vector format for area calculation. The SW extents and equivalent volumes derived from PS and S1-A were compared and the area differences were used to compute the mean absolute error (MAE), RMSE, and mean absolute percentage error (MAPE).

Based on a reference water mask covering SW in the PS data, the histograms of the backscatter coefficients for VH and VV polarizations were evaluated, separately for water and non-water pixels and using Otsu defined thresholds, the SW was classified separately for each polarization.

3.3.7 Suitability of volume estimation: Real world application

After calibrating and validating the approach in §3.3.1-3.3.6 to estimate tank water volume, two application examples were evaluated: 1) estimation of tank contributing water volume at the

basin scale using only SAR S1-A and 2) a time-series analysis for a single tank from multi-sensor observations.

To test (1) with the aim of evaluating the suitability of SAR for SW mapping of tank dynamics using solely S1-A observations, a time-series of SW area was extracted using the method in §3.3.1. The monitoring period covered the NE monsoon season in 2015 and 2017 and the water dynamics of 559 tanks were assessed (see §3.2.4 and Appendix E). Total water volumes were estimated for tanks that received water during this period from the most suitable derived power models (see §3.3.2). Since not all tanks in the basin were studied and the dynamic process of tank filling (*i.e.*, tanks are known to fill multiple times in a season) are not captured by infrequent state observations, it was not possible to evaluate the magnitude of volume estimates in the context of basin-wide precipitation totals. Instead, the TanDEM-X DEM (for the sample of testing tanks) were used to simulate fill levels to provide an approximate assessment of the volume estimates in the absence of field measurements. This simulation was achieved by modelling the water volume for the 72 tanks (see §3.3.2) at four stage levels (0.75, 1.5 m, 2.25 m, 3 m). From the sample of 72 tanks, for the tanks that filled in both years, the net volumes were calculated from the modelled DEM water levels. The estimate was also up-scaled to the full number of the of tanks, for the same tanks that filled in both years. For test (2) – the time-series application example – a high spatio-temporal resolution monitoring approach was investigated using a dense time-series analysis for a single tank from multi-sensor observations.

3.4 Results

3.4.1 Validation of bathymetry and SW area

Summary statistics for the error of the TanDEM-X DEM compared with the four field-surveyed tanks are shown in Table 3.4. The MAE and the RMSE between the TanDEM-X DEM and field elevations range from 0.67-0.86 m and 0.98-1.47 m, respectively for the four tanks. These vertical errors of the DEM are below the reported accuracies of 2–4 m, providing confidence for implementing the TanDEM-X DEM to derive V-A relationships for a larger sample of tanks (Eineder, Fritz, Abdel Jaber, Rossi, & Breit, 2012). The *a* and *b* parameters derived from the field data and the TanDEM-X DEM noted in Table 3.4 are also similar. The slight differences between the two data sources can be explained by Figure 3.5 which shows that the largest deviation in volume estimates between the two DEMs is at the bund area (heights > 4 m).

Table 3.4: MAE, standard deviation, RMSE, V–A relationships and the R^2 value for four tanks comparing the TanDEM-X DEM to topographic field measurements made in 2016.

Site	**Mean Absolute Error (m)**	**Standard Deviation (m)**	**RMSE (m)**	**Area Storage Relationship**	
				$V = a \times A^b$ **from field (F) & TanDEM-X (T) data**	**R^2**
Tank 1	0.67	1.22	0.98	(F) $V = 0.00061 \times A^{1.660}$ (T) $V = 0.00042 \times A^{1.693}$	97.35 97.34
Tank 2	0.86	1.72	1.47	(F) $V = 0.00107 \times A^{1.651}$ (T) $V = 0.00156 \times A^{1.542}$	90.32 95.83
Tank 3	0.76	1.12	0.89	(F) $V = 0.00021 \times A^{1.601}$ (T) $V = 0.00035 \times A^{1.590}$	93.78 91.89
Tank 4	0.80	1.50	1.26	(F) $V = 0.00861 \times A^{1.212}$ (T) $V = 0.00876 \times A^{1.251}$	96.42 95.33

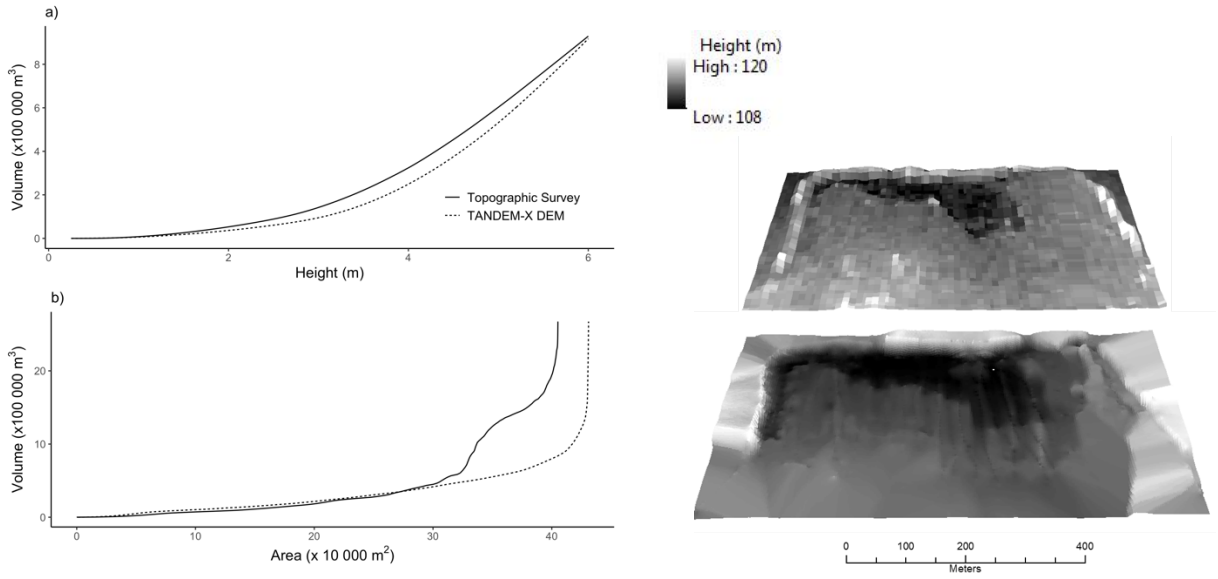

Figure 3.5: TanDEM-X DEM compared to the 2016 field DEM for tank 1. (a) stage height volume curve, (b) area volume curve, and (c) 3-D visualization of TanDEM-X DEM (top) and field DEM (bottom).

For the SW area extraction methodology, the classification derived from the VV polarized image had a stronger correlation with the reference water mask compared with the VH polarized image (96 % compared to 91 %) confirming a higher sensitivity of the VV polarization to the presence of SW in tanks. Furthermore, the effect of the backscatter incidence angle on the backscatter coefficient was tested for a collection of pixels located over SW and found no strong or significant correlation (see Appendix F, Figure F2).

With respect to the SW area, Table 3.5 shows the SW area (8.55 km^2) estimates of 111 tanks obtained from the PS images and from S1-A images in 2017. These tanks were selected such that they contained water on the observation dates. It was found that the classification of S1-A underestimates the total SW coverage by ~27 % (2.28 km^2) (Table 3.5). When comparing the SW estimates at the tank level, the MAPE varied substantially across the 111 tanks (Figure 3.6). SW estimates from S1-A had an RMSE of 30,540 m^2, equivalent to 27,741 m^3 for volume (Table 3.5). The average MAPE was 37.84 % and 45.71 % for SW area and volume, respectively. The high

MAPE for SW area is concerning because this error will translate to an even higher percentage volume error, since reservoir area and volume are related through a power relationship. To better understand the large MAPE between the PS and S1-A observations, the tanks with a MAPE above 30 %, which included 58 tanks (52 % of the sample) were visually inspected. The 13 tanks with a MAPE above 70 % revealed the same scenario (Figure 3.7a-d). These tanks showed elongated narrow SW extents in the PS imagery (Figure 3.7a). As a result, the SW areas were under detected in the S1-A imagery (Figure 3.7d), due to the spatial resolution of the sensor, and in turn caused high MAPE and an underestimation of the SW extent. Tanks with moderate MAPE (30-70 %) either contained a less severe case of the above underestimation (Figure 3.7e-h) and/or commonly displayed undetected water pixels around the border of the SW extent in the PS scenes (Figure 3.7i-l). These differences in tank SW extent and the total surface of inundated area comes mainly from the difference of spatial resolution between the two satellites and complexity in the S1 polarization response for SW detection. PS has a spatial resolution three times greater than S1 and therefore potentially captures increased detail. With regards to SAR imagery for small reservoir monitoring, there is large variability in backscatter intensities from water surfaces. The roughness of the water is highly variable and influences backscatter intensities over time and space. Difficulties also arise when the contrast between land and water deteriorates, due to the absence of vegetation on the land surrounding a small reservoir at the end of the dry season (Liebe, Giesen, et al., 2009).

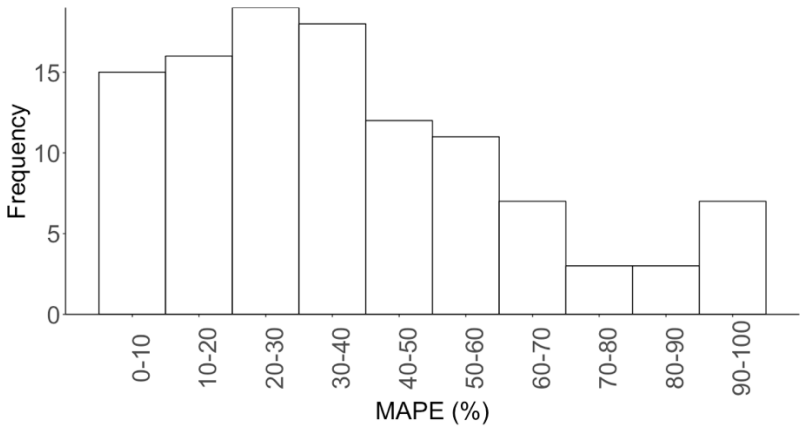

Figure 3.6: Histogram of MAPE for SW areas in 111 tanks.

Table 3.5: Accuracy of 111 tank SW extents and volume equivalents from S1-A and PS data.

Date	n	Total PS area (m^2)	Total S1A area (m^2)	RMSE (m^2)	RMSE (m^3)	MAE (m^2)	MAE (m^3)	MAPE (% Area)	MAPE (% Vol)
Sept. 2	34	2476863	1956500	23840	18864	19728	14266	33.17	40.86
Oct. 1	26	1719288	1411000	20151	14931	15261	10471	30.34	37.54
Oct. 8	51	4350330	2903000	38000	36388	30149	23970	44.78	53.11
All	111	8546481	6270500	30540	27741	23470	17835	37.84	45.71

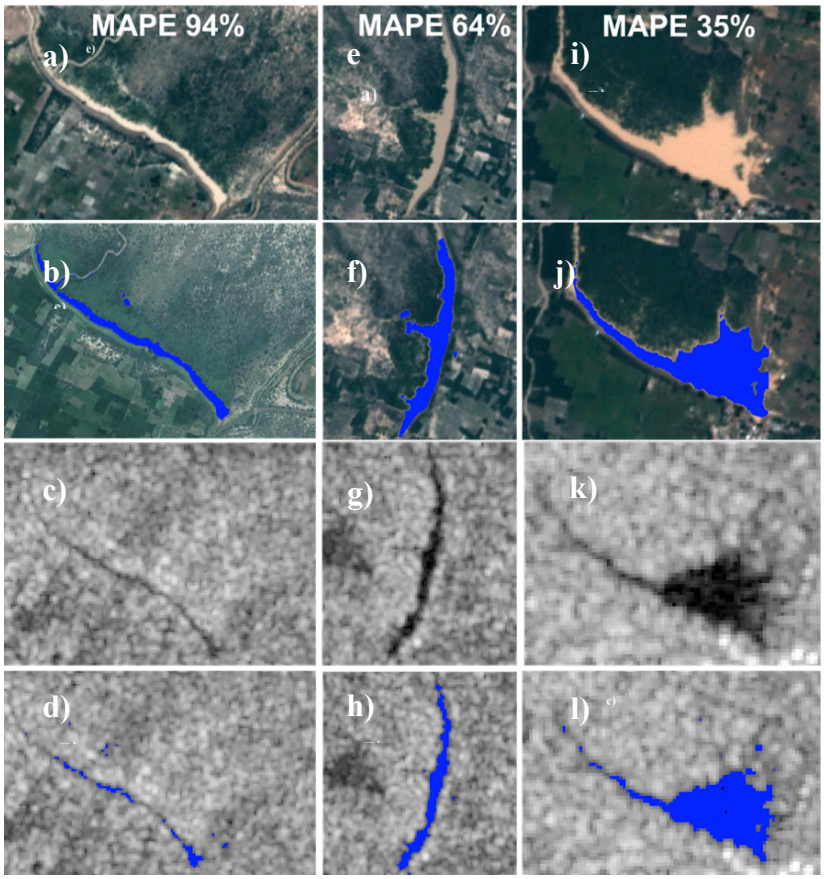

Figure 3.7: Examples of the MAPE for three tanks displaying variable MAPE % errors. (a), (e), (i) display PS true color composite (TCC); (b), (f), (j) show extracted SW area from PS on TCC image; (c), (g), (k) show S1-A scene; and (d), (h), (l) show extracted SW areas.

3.4.2 Understanding tank morphometry

The selected 72 tanks were representative of the various shapes and sizes of tanks that are present in S. India. Bund lengths (B_{len}) ranged from 599–3399 m (mean = 1305 m). Max tank volumes (V_{max}) ranged from 50445–809678 m^3 (mean = 243563 m^3). Low statistical associations (*i.e.* $R < 0.70$) were found between V_{max} and B_{len}, S_1, *b*, *a*, and A_{max} , and also between S_I and B_{len}, *b*, *a*, and A_{max}.

For Eq. 3.1, V-A coefficients *b* and *a* reveal information about the slope of the reservoir (the bund) and the openness of the half-pyramid tank bed, respectively. These parameters varied

significantly among the 72 tanks, with the *b* parameter ranging from 1.09–1.90 (mean = 1.46) and the *a* parameter ranging from 1.64E-05–1.57E-01 (mean = 1.30E-02). Of the 72 tanks, 45 (63 %) have *b* parameters that were < 1.5, indicating that tanks tend to have more concave bathymetries (Magome et al., 2003). The small *a* parameters for the 72 tanks reveal that the tanks are narrow and without an evident flat middle area (Magome et al., 2003). Although these tank structures primarily do have a flat bed, the main depressed region is present along the bund, from which the V-A relationship is developed. A correlation value (R = 0.98) was observed between the *a* and *b* parameters indicating a strong relationship. This high correlation between the parameters of the A-V relationships for the basin demonstrate that generic or category power equations obtained can be used with confidence.

3.4.3 Tank empirical storage relationship(s)

The V–A relationships for the tank categories (CAT) and by all tanks (GEN) are shown in Table 3.6. Despite the variety of reservoir sizes, the generalized equation for the 72 tanks fitted the observed model well with an overall R^2 of 95 %. The parameter values of the generalized V–A relationship (GEN in Table 3.6) for the Gundar Basin are in the same order of magnitude as those obtained for basins in Africa by Annor et al. (2009) and Liebe et al. (2005) for the Upper East Region of Ghana and by Sawunyama et al. (2006) for the Limpopo Basin in Zimbabwe. The power equations reported in these studies are from 41, 21, and 12 reservoirs and fitted the data with *b* coefficients of 1.44, 1.44 and 1.33, respectively. Young et al. (2017) found higher *b* coefficients of 2.1 and 2.0, respectively when investigating only two tanks. In our study, high *b* coefficients greater than 1.8 were obtained for three TS models in the sample of 72. Similar to our study in terms of reservoir size and a large sample size, Rodrigues and Liebe (2013) used a power

relationship to generate a and *b* parameters for 103 small reservoirs (1–40 ha) in two semi-arid watersheds. They also noted a high R^2 between the *a* and *b* parameters.

Table 3.6: Generalized V–A relationships and the coefficient of determination (R^2) values for GEN and CAT models. V is the tank volume (m^3), A is the tank surface area (m^2), and *a, b* are parameters.

Tank Size Category (CAT)	n	$V = a \times A^b$	R^2
<10	24	$V = 0.00277 \times A^{1.50}$	94%
10-20	24	$V = 0.00599 \times A^{1.41}$	96%
20-50	17	$V = 0.00734 \times A^{1.38}$	97%
>50	7	$V = 0.01116 \times A^{1.32}$	95%
All (GEN)	72	$V = 0.00871 \times A^{1.37}$	95%

3.4.4 Assessment of volume error

While the power relationships in Table 3.6 all fit the input data well, the sensitivity of the *a* and *b* parameters to the corresponding volume estimates is unclear. To assess this sensitivity, the V_{ERR} (%) of volumes estimated from the three models (TS, CAT, GEN) were compared with actual volume estimates from the DEM (Table 3.7, Figure 3.8).

Figure 3.8 and Table 3.7 show that in general, the CAT model had the lowest average V_{ERR} for each size category and fill level (h_{max}, 80 % and 50 %) and performed best. While the local TS model was expected to have the lowest V_{ERR}, it also appeared to introduce large uncertainties of volume estimation for select tanks. The basin-wide GEN model was similar in performance to the TS model. Consistently, the tanks in the smallest size category (<10 ha) and largest size category (>50 ha) had the highest V_{ERR} for all models. It should be noted, however, particularly for the GEN model, that the V_{ERR} is highly variable between the tank size categories, with the largest average V_{ERR} of 22.12 % for tanks <10 ha in size. The increased V_{ERR} for very small tanks is expected

because they vary substantially in shape. Understanding the higher V_{ERR} values associated with large tanks require a larger sample size.

The *a* and *b* parameters developed for the TS, CAT, and GEN models were originally developed at a h_{max} of 3 m. Evaluating the V_{ERR} at 80 % of h_{max} and 50% of h_{max} shows that the V_{ERR} largely decreases with fill level. This decrease is most evident at 50% of max where the V_{ERR} drops from 13.67 % to 6.84 % for the TS model. This is highly informative to the practical application of the power regression equations for volume estimation in tanks because water levels are rarely elevated to 3 m and thus the uncertainty in the estimates is likely closer to the V_{ERR} at the 80% and 50% cases.

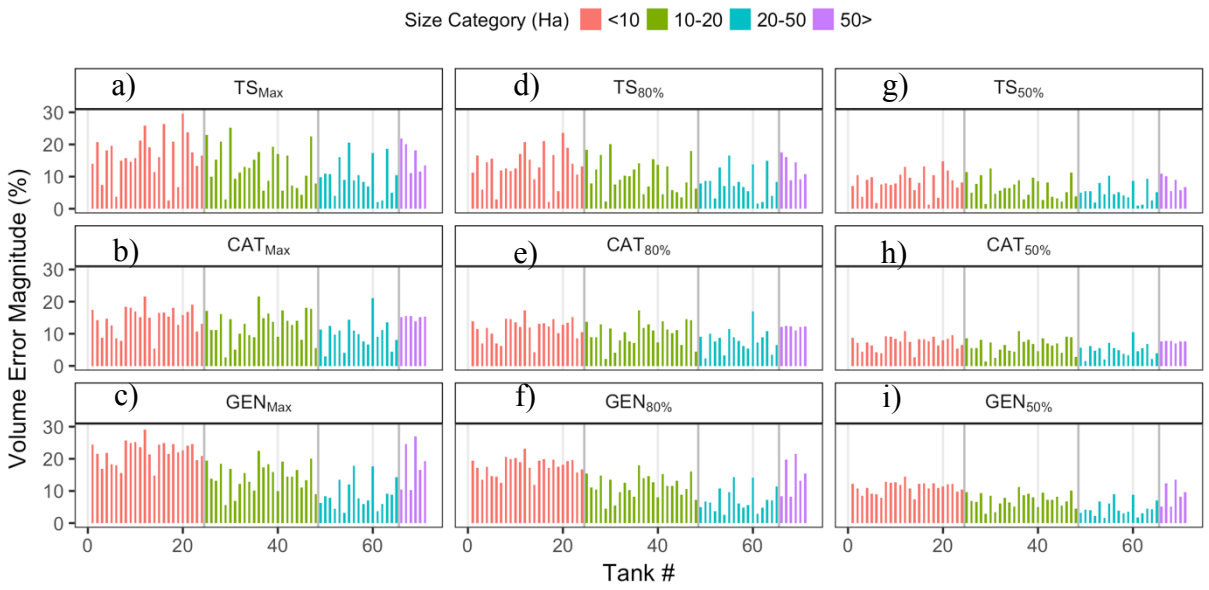

Figure 3.8: Volume (V_{ERR}) error from each tank using the three different models (a–c) at h_{max}, 80% of h_{max} (d-f) and 50% of h_{max} (g-i). Bars are colour coded by size category as per the legend at the top of the figure

Table 3.7: V–A model performance comparisons based on the mean (± standard deviation) percent volume error magnitude (V_{ERR}). "n" is the number of tanks studied in each size category. V_{ERR} 80% and V_{ERR} 50% refer to the volume error at 80% and 50% of h_{max} respectively.

Tank Size (ha)	n	TS			CAT			GEN		
		V_{ERR} max	V_{ERR} 80%	V_{ERR} 50%	V_{ERR} max	V_{ERR} 80%	V_{ERR} 50%	V_{ERR} max	V_{ERR} 80%	V_{ERR} 50%
< 10	24	16.5±6.8	13.2±5.5	8.2±3.4	14.5±3.9	11.7±3.1	7.3±1.9	22.1±3.4	17.7±32.8	11.1±1.7
10-20	24	12.8±6.4	10.3±5.1	6.4±3.2	12.6±4.6	10.1±3.7	6.3±2.3	14.4±4.3	11.6±3.4	7.2±2.1
20-50	17	10.1±5.4	8.1±4.3	5.0±2.7	9.9±4.3	7.9±3.5	4.9±2.1	9.0±4.1	7.2±3.6	4.5±2.2
>50	7	16.0±4.6	12.8±3.7	8.0±2.3	15.1±0.6	12.1±0.5	7.5±0.3	17.9±7.0	14.3±5.6	8.9±3.5
All	72	13.7±6.6	10.9±5.3	6.8±3.3	12.8±4.5	10.2±3.6	6.4±2.2	16.0±6.6	12.9±5.3	8.0±2.3

3.4.5 Assessment of remote sensing monitoring water availability in small reservoirs

The efficacy of measuring volume using solely SW extent and power models provides confidence in the applicability of RS SW extent to characterize tanks in remote regions and improve our understanding of water availability at various spatial scales. This sub-section demonstrates the results of our investigation with two tested application examples. The first application, test (1), presents the results for maximum water volume estimation at the basin scale for the 559 tanks using only SAR S1-A data for two high precipitation NE monsoon years (2015 and 2017) and the second, test (2), focuses on a time-series analysis for a single tank from multi-sensor observations.

Focusing on SW area changes during the NE monsoon, only 49 % (n = 274 based on 16 S1-A scenes) and 48 % (n = 268 based on 28 S1-A scenes) of the tanks showed water presence during the NE monsoon season. This highlights the first difficulty with attempting to contextualize our retrieved total volume estimate and tank dynamics (S1A-observation based). Despite good monsoon years, not all tanks are functioning and retained water, for example 177 of the same tanks showed no water presence for both years. This is not surprising as the literature highlights that

many tanks are currently not operating as functional structures able to retain water (Van Meter et al., 2016).

Using the power models based on size (*i.e.,* CAT) to estimate water volume observed at maximum fill for tanks with water present during the season, the SAR S1-A estimated volume is 8222995 m^3 and 5129576 m^3, respectively for 2015 and 2017. These estimates are difficult to compare as not all the same tanks filled in the two years. For this reason, the estimated maximum volume for the same tanks (n = 179) that received water for both observation years are reported. This revealed that between the two observations years, the total tank water volume was larger 36% for 2015 than 2017 (6303091 m^3 versus 4011419 m^3 respectively). This finding is supported by NE monsoon precipitation estimates for 2015 and 2017. The gridded Climate Hazards Group InfraRed Precipitation with Station (CHIRPS) satellite product data, showed total NE monsoon precipitation for 2015 was 596 mm compared with 282 mm for 2017. To evaluate what these net volume estimates mean in the context of tank filling, the net estimates for the 179 tanks were compared against our simulated four filling cases representing the potential maximum fill at each stage level. As noted in §3.3.7, this process was done for the full 179 tanks and the subset of the 179 tanks that corresponded to the same tanks for each year from the sample of 72, which resulted in 34 tanks. The simulated fill levels from the 34 tanks were estimated directly from the DEM. The simulated fill levels for the 179 tanks were estimated from the DEM for the sample of 72 tanks. Within the sample of 72 tanks, the median volume for each size category was calculated for each fill level, resulting in one volume estimate for each size class: < 10 ha, 10-20 ha, 20-50 ha and > 50 ha. The 179 tanks were labelled with one of the former noted size categories and in turn, with a median volume estimate. The sum of the 179 tanks based on the median volumes was subsequently calculated for each fill level. While the 34-tank simulation is more accurate, it is only

a small subset and therefore, the 179-tank median net volume estimates were also considered. As shown in Figure 3.9, compared to simulated tank filling levels, estimated tank volumes from the power relationships for both years showed tanks filling closest to simulated stage level category of 1.5 m; they did not fill close to full simulated capacity (set at a stage of 3 m in this work).

Both the observed years are an underestimation of the total input to the basin's water budget since functioning tanks can fill multiple times, water is lost through the system and many hydrologic processes are not captured by infrequent state observations from space. However, the fact that the 2017 estimated fill levels were lower than the 2015 levels agrees with the lower basin-wide precipitation in 2017 estimated from the CHIRPS data.

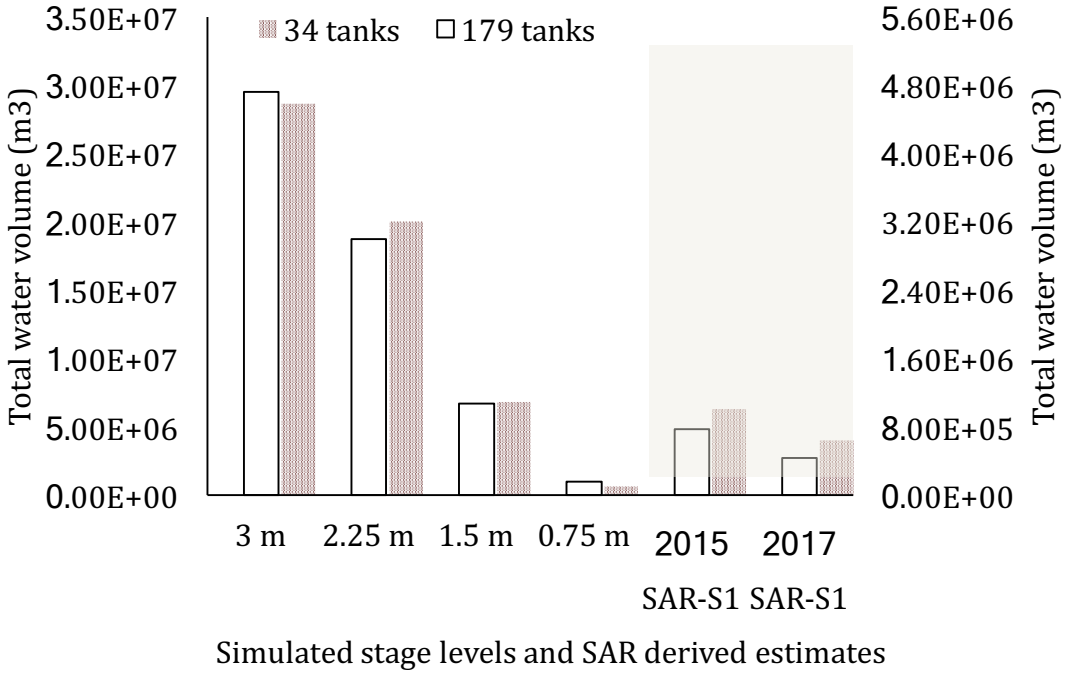

Figure 3.9: Total water volume for 179 tanks (DEM median based) and 34 tanks (DEM only) with simulated fill levels at 3.0 m, 2.25 m, 1.5 m and 0.75 m using the TanDEM-X DEM and compared with SAR 2015 and 2017 estimates.

While the volume estimates retrieved using S1-A over larger spatial scales provided insight into the maximum water extent and potentially the stored water volume, the temporal sampling of the tanks by S1-A alone is likely not good enough to evaluate the tank volume changes over time. Therefore, for test (2), a time-series of satellite-based volume estimates was calculated and shown for a selected tank in Figure 3.10. This tank and observation year provides an example of a season with both cloud-free optical observations (PS, S2 and L8) and S1-A data, for a NE monsoon season. The tank has a maximum SW area between 10-20 ha and therefore, the CAT 10-20 ha equation from Table 3.6 is used as the power model to retrieve volume estimates. All cloud-free observations from optical and SAR sensors covering the tank were retrieved for the period between August 2017 and January 2018.

The volumes shown in the main graph of Figure 3.10a were retrieved from cloud-free observations while the coloured markers above the graph in Figure 3.10a correspond to scene acquisition dates, regardless of cloud contamination. This clearly shows the unavoidable challenge with employing optical RS observations for monitoring as they are often not useable due to cloud presence. While PS imagery is subject to variable cloud contamination, its high temporal resolution enables more frequent cloud-free observations than L8 and S2 sensors and facilitates not only a single snapshot of the volume but the seasonal variation of tank water volume. PS provides 27 SW areas, compared to three, four and 12 from L8, S2, and S1, respectively. Water volumes in the tank rose sharply at the start of September following the monsoon rains, and then dropped over the next three months as water was discharged from the tank (Figure 3.10a). Figure 3.10b-c show the tank on September 2 observations from PS and S1-A, corresponding to the largest SW area of the tank for this season. While a full water balance explanation for the varying change in volume from tank to tank, or for the tank shown here is beyond the scope of this research, this

application test highlights how the combination of satellite radar and frequent visible-infrared observations of can be used to monitor tanks regularly all year-round. Additionally, inferences about inflows and outflows can be made if multiple adjacent daily observations are available.

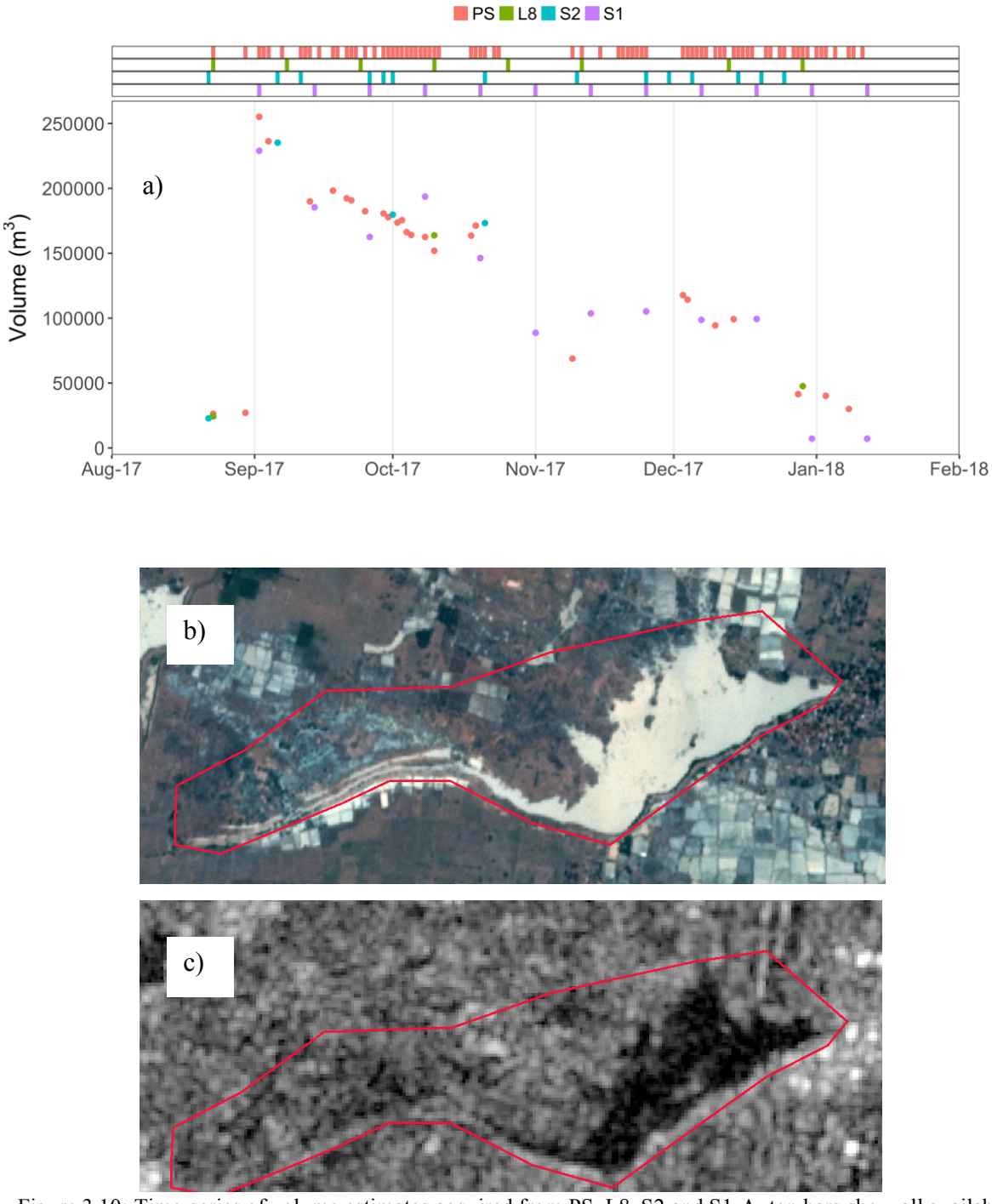

Figure 3.10: Time-series of volume estimates acquired from PS, L8, S2 and S1-A, top bars show all available acquisition dates while the dots for each sensor show only the volume retrieved from cloud free observations. b-c show b) PS TCC image and c) S1-A VV polarized.

3.5 Discussion

In this study, power relationship(s) were used to estimate tank water volume in the Gundar Basin, India for the calculation of net storage at the basin scale and monitoring changes in volume at the tank scale using TanDEM-X DEM data. This dataset provided an opportunity to evaluate V-A relationships for water volume estimation covering a sample of tanks (n = 72). Based on the application of the V-A relationship method applied to 72 tanks, volumes can be estimated within an absolute volume error range of 6-8 % (TS, GEN and CAT models) for water levels below 1.5 m, with the CAT model providing the best solution according to the V_{ERR} method. The application of SAR observations for water monitoring has a developed history (Bolanos et al., 2016; Musa et al., 2015; Xie et al., 2015), but this is the first study using S1-A to monitor SW area changes for tanks in S. India. The PS data were invaluable for both augmenting the observation frequency of S1-A to continuous (~1 day) monitoring (Cooley, Smith, Stepan, & Mascaro, 2017) and for validation of SW area. When the S1-B data is available for our study region, temporal monitoring will increase potentially to 6 days. Beyond this, the C-Band RADARSAT Constellation Mission (RCM) planned for launch in 2019 will offer advanced capabilities for monitoring SW with high spatial resolution and temporal resolution, providing enhanced monitoring of tanks during the monsoon seasons.

While TanDEM-X DEM data produced V_{ERR} between 10-20 %, currently it is the only feasible dataset to implement to retrieve tank topography at large spatial scales. By indicating the uncertainly for volume estimation, users implementing our method can evaluate if the specified error is acceptable. While the bathymetric field data supported the use of TanDEM-X DEM data, it is unknown if this is the case for tanks in the lower basin because the monsoon regime is typically variable across the basin. Since the TanDEM-X DEM is from RS observations

spanning a five-year period, some scenes incorporated in the generation of the DEM may have been acquired when tanks contained water, contributing to differences in bathymetry values (Collins, Riegler, Schrader, & Tinz, 2015). To better understand these differences due to water presence, a bathymetric survey should be completed on a larger number of tanks in the middle and lower basin.

To improve the accuracy of extracting the SW area from the S1-A images, the incorporation of a shape metric (S_I) as a metric to eliminate SW areas that are too narrow to be accurately detected is suggested. In this study a tank mask was used to reduce errors in the estimation of SW area using S1-A; however, to apply the volume estimation method to a larger number of tanks, either a vector dataset of tank boundaries is needed or the methodology for SAR SW estimation needs to be improved to ensure that only open water areas are detected. The latter is a non-trivial problem because when water pools start forming in the fields surrounding the tanks, the land-water contrast deteriorates causing problems for tank SW area extraction (Eilander et al., 2014). In addition, before S1-A imagery can be fully implemented into a larger-scale hydrological observing system for tanks, the influence of water surface roughness and vegetation presence on backscatter intensity needs to be understood; these can affect the error in SW delineation (Annor et al., 2009). By resolving these issues, it should be possible to use S1-A for continuous SW area monitoring to inform water management decisions.

Finally, it is noted that power law type expressions can be used as effective storage-discharge model predictors for the hydrologic modelling of tanks. Unlike other studies using generalized power law expression for volume estimation (Annor et al., 2009; Sawunyama et al., 2006), this study shows that the *a* and *b* parameters are spatially variable and that volume estimates are sensitive to these parameters. When combining the power law expressions and SW estimates,

the ability to understand the dynamic amount of water stored in the region or in a large hydrological unit for managing local water resources was highlighted. With over 160,000 of these structure present in S. India, the hydrological potential of these systems to store water managed use is extremely important. This could have significant societal benefit by improving the prediction and application of irrigation in marginalized rural communities in S. India who are unable to cope with climate extremes. In the future, water volume extraction methods noted in this work could be incorporated into a hydrological and crop management framework to evaluate water requirements under current and future climate scenarios. Additionally, the Surface Water and Ocean Topography (SWOT) mission, to be launched in 2020, should be able to provide the first application of satellite altimetry for tanks and could be incorporated into our tank monitoring methodology by providing water levels at a higher temporal and spatial resolution.

3.6 Conclusion

Tank systems are a potential solution for reducing water stress in S. India by providing local groundwater recharge and a means of storing surface-accessible water for longer durations during the dry seasons. In this study, it is shown that RS techniques can be an important tool for tank monitoring providing an opportunity to understand the dominant hydrologic controls governing reservoir outflow and inflows. A methodology is developed to monitor and quantify water volume in tanks under all weather conditions for tanks in S. India, using high quality S1 SAR observations, freely available online, and high-resolution PS data. Our results coupling empirical V-A models and remotely sensed SW area is a promising first step and proof of concept toward future modelling of ungauged flows in tanks, especially as developments in cloud computing for RS make our method easily applicable to any basin. The ability to estimate reservoir volumes using satellite RS has wide reaching implications in transboundary water management. If

equipped with remotely sensed observations of tank volumes, stakeholders can make more informed decisions about a wide array of water management issues related to tank use. RWH tank systems are currently not continuously monitored and thus, our findings represent a unique contribution to the hydrologic science community.

Acknowledgments: The authors acknowledge the support from the Natural Science and Engineering Council's Discovery Grant program, seed funding from the University of Waterloo's International Research Partnerships Grant, and from DLR (Germany) for access to TanDEM-X DEM data under the successful proposal DEM_HYDR0751.

Chapter 4

Discussion

4.1 Summary and Contributions

Characterizing the seasonal variation of freshwater is critical for ensuring sustainable use of water resources and therefore, the ability of biological systems to support human needs. This is especially true in S. India, where water resources are limited, unequally distributed in space and time and vulnerable to changes in climate, and where societies are dependent on surface waters for their livelihoods. The study presented in Chapter 3 identifies how space-based observations of SW distribution in the Gundar basin can improve our understanding of water availability at various spatial scales. Limited in several respects, the first application of SAR observations and a high-resolution global DEM for tank monitoring provide a proof-of-concept for monitoring tank structures using RS techniques.

At the onset of this thesis, three operational goals were established that have been addressed throughout the course of this study. The first finding of this thesis, though small, is significant; for the first time, tank bathymetry can be retrieved from a high-resolution global DEM. The most accurate 'modelled' estimate of tank SWS is, in theory, calculated directly from tank bathymetry (for all tanks). Even though the TanDEM-X DEM does provide full spatial coverage, the bathymetry of many tanks was not captured because of vegetation issues in the tank bed or water presence shown in the WIM. Fortunately, it was found that the bathymetry for a large subset of tanks can be retrieved using TanDEM-X DEM based on low WIM frequency values and visual inspection. The application of the TanDEM-X DEM was crucial to provide the ability to develop

empirically-derived tank storage relationships for a large sample of tanks (n = 72). As noted previously in Chapter 2 (see Table 2.1), although SWS has been estimated in small lakes and reservoirs with the combination of radar altimetry, visible-infrared reflectance and radar backscatter data, no prior work has focused on monitoring tank SWS during the monsoon season. Prior to the availability of TanDEM-X DEM for the retrieval of V-A power models, tank SWS was evaluated ten years prior by examining the spectral response of water from Landsat reflectance observations to approximate water depth (Mialhe, Gunnell, & Mering, 2008). While this work was critical to set the foundation and discussion surrounding the application of EO to support understanding of tank rehabilitation, their method does not allow monitoring during critical monsoon – habitually cloud covered – periods or when tank water is turbid. Furthermore, the field of satellite RS has witnessed a significant expansion of EO platforms for terrestrial water monitoring (McCabe et al., 2017); a clear example of this technological advancement has been illustrated in Chapter 3 from the ability of a satellite derived DEM (*i.e.*, TanDEM-X DEM) to measure detailed geometry of tank structures (Mialhe et al., 2008).

The TanDEM-X DEM product has set the foundation for evaluating simple, commonly applied, power type expressions for volume estimation in small storage structures (Karran et al., 2017; Liebe et al., 2005; Meigh, 1995; Sawunyama et al., 2006; Young et al., 2017). To achieve the second operational goal, this research built on the success of the previous studies to evaluate the suitability of empirical power law expressions for water volume estimation in tanks. At the individual tank scale (*i.e.*, TS model), the results present significant power relationships between the storage and area for the 72 tanks – a predicted result, given the success of the previous studies and the expected over-fitting of the model when focused on independent tank structures. More interestingly, and perhaps unpredictable, is our result showing high variability for a and b

parameters among the 72 evaluated tanks and the substantial impact this variability introduces to volume estimates. It is an unpredictable result because common practice has been to develop a single regionalized V-A equation for geomorphological similar landscapes, with the latter point lending to the assumption of minimal variation among reservoirs. Results in Chapter 3 highlight that variability among individual structures, even in geomorphologically similar landscapes, is important to consider when determining 1) the suitability of a power type relationships and 2) assessing a baseline to compare volume estimates when further approximating the models (*i.e.* CAT and GEN). Likely, previous studies have been unable to evaluate the former points due to limited bathymetric data. Fortunately, the TanDEM-X DEM facilitates the calculation of a dense set of bathymetric data for tanks, providing the ability to generate four power type models for volume estimation in tanks. Prior to this research there was no RS-based method to estimate SWS in tanks during monsoon periods: this is now possible with power law tank expressions and with estimated volume uncertainties.

The two application test examples, volume estimation using the derived power models combined with multiple satellite observation-based SW extent, shows promising application of SWS monitoring. A detailed history can now be built regarding tank volume changes and when up-scaled to several tanks in the same cascade, management and water use questions at the cascade level can be addressed. Furthermore, tank volume estimates could now be used for a variety of applications. For example, Liebe et al. (2009) showed that small reservoirs can be used as runoff gauges by monitoring their surface area with remotely sensed time-series and regional V-A relations. In addition, when combined with precipitation records, remotely sensed reservoir storage changes can be used to calibrate a simple hydrological model (Liebe, Van De Giesen, et al., 2009).

These are potentially powerful practical applications of the proof of concept developed in this thesis.

4.2 Methodological issues and limitations

The methodology used in this study has several limitations. Here, the discussion is divided by limitations and uncertainties within the confines of 1) input data and 2) user-defined methodology.

4.2.1 Data related limitations

The primary limitation of using RS and model outputs is that the resolution (spatial and/or temporal) of the sensing system may not sufficient for the hydrological analysis. Results from this thesis indicate the water dynamics of tank structures cannot be captured solely with S1-A at the temporal resolution of 12 days. While S1-B is operational and increases the observation to a six-day period, S1-B does not acquire observations over the study region. With respect to spatial resolution, lower agreement between S1-A extracted SW extent and PS-estimated inundation areas showed that where water accumulates along a spatially constrained area, such as a narrow SW area near the retaining wall, even currently available high spatial resolution SAR data (*i.e.*, 10 m) may not (yet) be sufficient to capture SW extent. A similar issue is noted by Ottinger et al. (2017), who mapped aquaculture ponds using S1-A and found the spatial resolution of the data limiting to the applicability of the observations to accurately recover pond outlines (Ottinger et al., 2017). Furthermore, the developed power regression models are limited by spatial resolution, and spatial and height accuracy of the bathymetry estimation. While the TanDEM-X DEM dataset is an improvement over SRTM and other global satellite DEMs and can capture tank bathymetry, it is still a modelled approximation of the real-world terrain with errors and

uncertainties caused in many cases by insufficient spatial resolution. A limitation in the DEM accuracy also relates to tank processes which can influence the InSAR DEM estimation accuracy. For example, tank bathymetry, and volume estimation, is altered when silt is removed from the tank for agricultural applications and vegetation encroachment in tank beds (Gunnell, Anupama, & Sultan, 2007; Sato, 2013). These dynamic factors change over-time and continue to introduce additional error to the volume estimate using the methodology developed in this research. Although the error was difficult to evaluate and account for in this research due to time constraints, it could be undertaken in future. Nevertheless, no other DEM or surface products are available to retrieve tank bathymetry and no other RS based methods are appropriate to measure water volumes in tanks, indicating that this study represents a contribution to this field of SWS monitoring.

Beyond the limitations related to tank bathymetry, TanDEM-X DEM has additional known inconsistencies and errors, particularly when applied for hydrological analysis. A hindrance with the application of the DEM is the unknown likelihood of water presence. While DLR provides the WIM along with the product, it is still a challenge to determine the uncertainty for landscapes with seasonal and not permanent water presence (Eineder et al., 2012). A high vertical agreement between TanDEM-X DEM and the total station topographic measurements confirmed confidence for tank bathymetric retrieval using the TanDEM-X DEM but this confidence is limited to a confined geographic location. It is possible that tanks in the lower basin do not present strong vertical agreement if *in situ* bathymetry was collected. This is only speculative and further study is needed to determine if there was increased water presence during scene acquisition for tanks in the lower basin. The clustering of the significant differences in elevation between the TanDEM-X DEM and *in situ* survey data primarily in the tank water spread area support that water presence

during scene equation does influence the bathymetry (Figure 4.1). Despite this, a study that developed a wet and dry season DEM from TanDEM-X data for small reservoirs in northeastern Brazil demonstrate that the retained water during data acquisition had little impact on the derived reservoir bathymetry and on estimated water volumes (Zhang et al., 2016). This should be verified with an increased number of field surveyed tank elevation measurements during the dry-season.

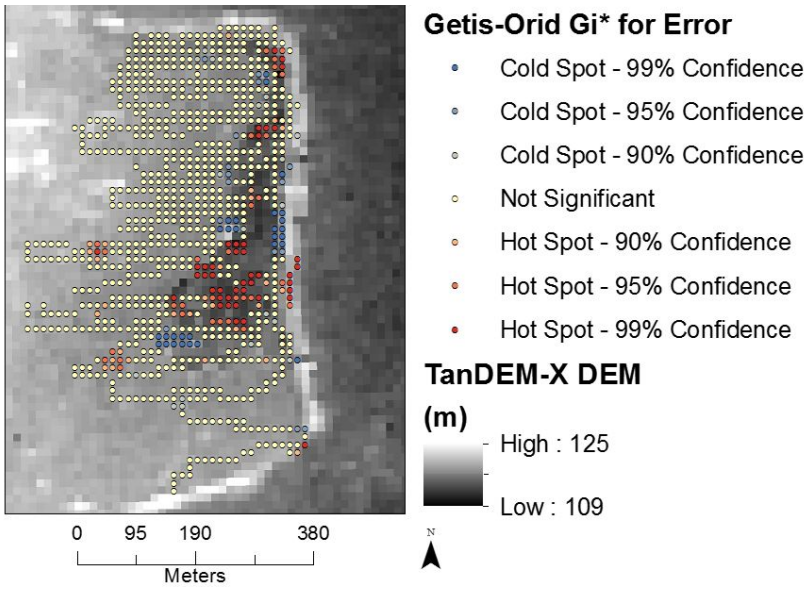

Figure 4.1: Spatial distribution of the Getis-Orid Gi* z-scores labelled as confidence level for elevation differences between TanDEM-X elevations and in situ data for a field surveyed tank. Hot spots are located primarily in tank water spread area.

4.2.2 User-driven methodological limitations

User-driven methodological choices also introduced uncertainty and limitations for this study. The first limitation is related to the reporting of uncertainty in Table 3.7. Uncertainties are identified for both the satellite-derived SW areas and the established power relationships statistically independent of one other. The uncertainties in the model-estimated water storage

volumes will however be larger because they will combine uncertainties from the SW area estimates and the volumes estimates from the V-A relationships.

The research area of accurate reservoir water boundary detection using SAR is still a debated topic in the literature and a challenging task (Amitrano et al., 2014; Eilander et al., 2014; Liebe, Van De Giesen, et al., 2009). The challenge is due to the large variation in the radar backscatter from water surfaces. While the Otsu method was efficient to implement in the GEE environment for unique tank and scene backscatter threshold selection, the method might not be a robust algorithm; a robust algorithm for SAR reservoir water delineation here is defined as one that can operate all year round and provide weather independent small reservoir monitoring. To date no such algorithm exists that is fully autonomous and accurate because of uncertainties arising from wind (e.*g*., surface scattering) and low land-water contrast at the end of the dry season. Therefore, the Otsu method is likely less robust for monitoring at the tail end of the season because there is no longer a bimodal distribution between water and non-water pixels (Otsu, 1979); other techniques might be more applicable (Bolanos et al., 2016; Eilander et al., 2014; Mueller et al., 2016). Although wind-induced surface scattering (*i.e.,* Bragg scattering) was not observed during the NE monsoon monitoring period, it was observed during the SW monsoon, which is the windy season (Figure 4.2). Extraction of SW area with VV polarized data on July 9th of 2016 would result is a large underestimation of the true extent as wind induced Bragg scattering has significantly increased the backscatter; this is not observed in the HV data (Figure 4.2). While the impact of wind induced Bragg scattering was minimal during the NE monsoon season (observation period in Chapter 3) and the VV co-pol derived SW extents were in higher agreement with PS extracted SW extents, co-pol (VV) and cross-pol (VH) data should be combined for improved SW detection when moving to year round tank monitoring.

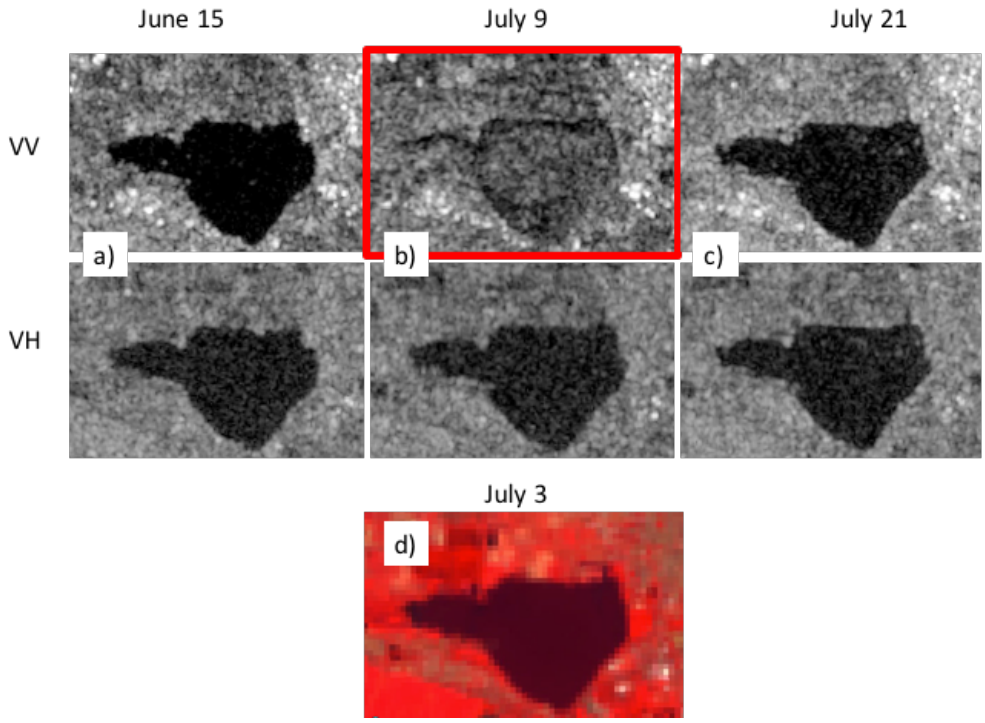

Figure 4.2: VV and VH channels over a tank reservoir, showing better land–water discrimination with the cross-polarization channel when windy (July).

While the GEE was, and will continue to be an extremely valuable platform for efficient satellite data access and analysis, there was a trade-off in time when performing analysis. GEE is a programming interface and for S1 data, there is currently very few pre-existing algorithms, such as speckle filters, that have been translated into the JavaScript code environment. Therefore, the availability of an API presents a trade-off between the ease-of-use for a user and the flexibility to implement complex functions within said API. From this research, a workflow has been developed to continue SW extraction from L8, S2 and S1-A over tanks. The challenge still lies in automating the processing of the PS data and ingesting the data efficiently into the workflow. The time-series analysis using PS was presented for a single tank and the imagery was selected to contain minimal cloud cover and subsequently, SW extent was visibly checked to verify automated SW extraction performed well on all imagery. This was a manual process and needs to be improved before PS

data can be utilized for the large scale hydrological analysis of tanks. This is in agreement with Cooley et al. (2017), who notes many of the challenges that persist in PS data for large-scale analysis including a lack of an automated cloud mask, geolocation inaccuracies, and inconsistent radiometric calibration across multiple dove satellites (Cooley et al., 2017).

4.3 Opportunities and future work

Despite the above limitations and challenges, specific methodological considerations can overcome some of them to improve the tank SWS methodology. First, SW extent extraction can be improved for year-round monitoring by combining the VV and VH bands. Furthermore, incorporating auxiliary temporal information would help to resolve errors introduced by low land water contrast during the tail-end of the season or on high wind acquisition days (Eilander et al., 2014; Liebe, Giesen, et al., 2009). As followed by Eilander et al. (2014), this work also utilized a mask of tank boundaries for the Gundar; to up-scale the analysis to the regional scale, a larger mask will need to be developed.

The most pressing and exciting opportunity moving forward is the automation of the method, considering the datasets used in this research but also in conjunction with the large volume of data for SW extraction available in the near future (Appendix C). Our research highlights that the temporal frequency of S1-A acquisitions alone (12 days) is insufficient to monitor the highly variable hydrologic water cycle (primarily output) of tanks. The time-series analysis does however highlight that there is sufficient EO optical datasets now available that can provide the required temporal resolution to begin to understand tank dynamics. While PS data is daily, cloud cover still presents a serious challenge when processing and utilizing the data at larger spatial scales. Moving forward, the RCM to be launched in 2019 will further increase the number of observations and will be a critical source of information for tank monitoring during the monsoon periods.

Beyond the increased number of SAR mission in the future, the SWOT mission (2020 launch) will present several new opportunities to understand tank SWS. SWOT will be the first altimetry dataset with a high enough spatial resolution to potentially retrieve water heights for tanks. This is turn would allow the evaluation of SWS storage estimated from satellite estimated SW extent and altimetry estimated H. While this research focused on the foundational methods to estimate SWS in tanks, moving forward, many interesting questions can now be addressed in subsequent work. With the tank volume estimation framework, a wide variety of novel experiments could be run to investigate tank dynamics. For example, a time-series for tanks within the same cascade can be developed to evaluate the timing of water release dynamics and if these dynamics are conducive to command area crop requirements. In addition, past multi-mission SAR data, dating back to the 1990s, can be incorporated to investigate long term change in tank SWS storage.

Chapter 5

Conclusions

This thesis asked the question: Can RS observations be used to monitor tank systems? The answer to this question is perhaps the greatest contribution of this thesis. A flexible framework for volume estimation in tanks has been created from available RS data. To date, few studies in the literature have focused on the ability to monitor tanks from space and no studies have investigated the monitoring of tank volume dynamics at the basin scale with the integration of radar and visible infra-red constellation sensor observations. Furthermore, although this research had the benefit of leveraging the TanDEM-X DEM, this resource at 12-m spatial resolution is not openly available to the public.

The study presented in Chapter 3 identified how space-based observations of SW distribution in the Gundar Basin can improve our understanding of water availability at various spatial scales. Although limited in some respects, the first application of radar observations and a high-resolution global DEM for tank monitoring provide a proof of concept in the context of monitoring the tank structures. The results demonstrate that S1-A SAR observations can be used to monitor tank water extent and when combined with power models fitted to tank bathymetry, time-series volume estimates can be calculated. When the Sentinel-1B data is collected for the region, the temporal scale of monitoring will increase from 12 days to 6 days. Since this data is freely available and can operate in all weather conditions, it is highly advantageous to use this system for systematic monitoring of small reservoirs. Beyond this, the synergy of optical data and SAR data is crucial; it increases temporal frequency but can also validate the SAR based water

retrieval estimates. Although cloud cover is a hindrance for the operational use of optical data in water monitoring applications, the high temporal daily revisit of optical constellation satellites provides an increasingly frequent series of cloud-free data during critical monsoon observation periods. While it is challenging to fully and comprehensively validate volume estimates, the results show strong potential to employ RS observations to further explore tank water dynamics at various spatial scales. Now, with power law type expressions and the uncertainty estimates, volume estimates in tanks between 5-80 ha can be estimated solely based on SW extent without the need for tank bathymetry.

Tank systems are a potential solution for reducing water stress in S. India by providing groundwater recharge and a means of storing water for longer durations. This research provides a stepping stone to understand these systems by providing a potential method to monitor water storage within tanks using satellite RS techniques. Tank systems are currently not continuously monitored and thereby, this research has offered a unique contribution to the hydrologic science community by incorporating SAR data and a high-resolution DEM for tank monitoring.

References

Amitrano, D., Ciervo, F., Martino, G. Di, Papa, M. N., Iodice, A., Member, S., … Ruello, G. (2014). Modeling Watershed Response in Semiarid Regions With High-Resolution Synthetic Aperture Radars. *J-STARS*, *7*(7), 2732–2745.

Annor, F. O., van de Giesen, N., Liebe, J., van de Zaag, P., Tilmant, A., & Odai, S. N. (2009). Delineation of small reservoirs using radar imagery in a semi-arid environment: A case study in the upper east region of Ghana. *Physics and Chemistry of the Earth*, *34*(4–5), 309–315. https://doi.org/10.1016/j.pce.2008.08.005

Aubriot, O., & Prabhakar, P. I. (2011). Water institutions and the "revival" of tanks in south India: What is at stake locally? *Water Altern.*, *4*(3), 325–346.

Baup, F., Frappart, F., & Maubant, J. (2014). Combining high-resolution satellite images and altimetry to estimate the volume of small lakes. *Hydrology and Earth System Sciences*, *18*, 2007–2020. https://doi.org/10.5194/hess-18-2007-2014

Behnamian, A., Banks, S., White, L., Brisco, B., Millard, K., Pasher, J., … Battaglia, M. (2017). Semi-Automated Surface Water Detection with Synthetic Aperture Radar Data : A Wetland Case Study. *Remote Sensing*, *9*(1209), 1–21. https://doi.org/10.3390/rs9121209

Bioresita, F., Puissant, A., Stumpf, A., & Malet, J. (2018). A Method for Automatic and Rapid Mapping of Water Surfaces from Sentinel-1 Imagery. *Remote Sensing*, *10*(217), 1–17. https://doi.org/10.3390/rs10020217

Birkett, C. M. (1998). Monitoring of Large Rivers and Wetlands (B), *34*(5), 1223–1239.

Birkett, C. M., Mertes, L. A. K., Dunne, T., Costa, M. H., & Jasinski, M. J. (2002). Surface water dynamics in the Amazon Basin: Application of satellite radar altimetry. *Journal of Geophysical Research Atmospheres*, *107*(20), 1–21. https://doi.org/10.1029/2001JD000609

Bitterman, P., Tate, E., Van Meter, K. J., & Basu, N. B. (2016). Water security and rainwater harvesting: A conceptual framework and candidate indicators. *Applied Geography*, *76*, 75–84. https://doi.org/10.1016/j.apgeog.2016.09.013

Bolanos, S., Stiff, D., Brisco, B., & Pietroniro, A. (2016). Operational surface water detection and monitoring using Radarsat 2. *Remote Sens.*, *8*(4), 285. https://doi.org/10.3390/rs8040285

Bonn, F., & Dixon, R. O. Y. (2005). Monitoring Flood Extent and Forecasting Excess Runoff Risk with RADARSAT-1 Data. *Natural Hazards*, *35*, 377–393. https://doi.org/10.1007/s11069-004-1798-1

Brisco, B., Kapfer, M., Hirose, T., Tedford, B., & Liu, J. (2011). Evaluation of C-band polarization diversity and polarimetry for wetland mapping. *Can. J. Remote Sensing*, *37*(1).

Brisco, B., Short, N., Van Der Sanden, J., Landry, R., & Raymond, D. (2009). A semi-automated tool for surface water mapping with RADARSAT-1. *Can. J. Remote Sens.*, *35*(4), 336–344.

Brown, G. S. (1977). The Average Impulse Response of a Rough Surface and Its Applications. *Trasactions on Antennas and Propagation*, (1), 67–74.

Cazals, C., Rapinel, S., Frison, P., Bonis, A., & Mercier, G. (2016). Mapping and Characterization of Hydrological Dynamics in a Coastal Marsh Using High Temporal Resolution Sentinel-1A Images. *Remote Sensing*, *8*(570), 1–17. https://doi.org/10.3390/rs8070570

Clement, M. A. (2018). Multi-temporal synthetic aperture radar fl ood mapping using change detection. *Flood Risk Management*, *11*, 152–168. https://doi.org/10.1111/jfr3.12303

Collins, J., Riegler, G., Schrader, H., & Tinz, M. (2015). Applying terrain and hydrological

editing to TanDEM-X data to create a consumer-ready worlddem product. *Photogramm. Remote Sens.*, *40*(7), 1149–1154. https://doi.org/10.5194/isprsarchives-XL-7-W3-1149-2015

Cooley, S. W., Smith, L. C., Stepan, L., & Mascaro, J. (2017). Tracking Dynamic Northern Surface Water Changes with High-Frequency Planet CubeSat Imagery. *Remote Sens.*, *9*, 1–21. https://doi.org/10.3390/rs9121306

Crétaux, J., & Birkett, C. (2006). Lake studies from satellite radar altimetry. *Applied Geophysics*, *338*, 1098–1112. https://doi.org/10.1016/j.crte.2006.08.002

Crétaux, J., Jelinski, W., Calmant, S., Kouraev, A., Vuglinski, V., Bergé-Nguyen, M., … Maisongrande, P. (2011). SOLS: A lake database to monitor in the Near Real Time water level and storage variations from remote sensing data. *Advances in Space Research*, *47*(9), 1497–1507. https://doi.org/10.1016/j.asr.2011.01.004

Dasgupta, S., Dwivedi, R. S., Kushwaha, S. P. S., & Bhattacharya, S. N. (2010). Monitoring the spatial extent of coastal wetlands using ERS-1 SAR data. *Int J Remote Sens*, *20*(13), 2509–2517. https://doi.org/10.1080/014311699211903

Degefu, D. M., Weijun, H., Zaiyi, L., Liang, Y., & Zhengwei, H. (2018). Mapping Monthly Water Scarcity in Global Transboundary Basins at Country-Basin Mesh Based Spatial Resolution. *Scientific Reports*, *8*(2144), 1–10. https://doi.org/10.1038/s41598-018-20032-w

Eilander, D. M., Annor, F. O., Iannini, L., & van de Giesen, N. (2014). Remotely sensed small reservoir monitoring: A Bayesian approach. *Remote Sens.*, *6*, 1191–1210.

Eineder, M., Adam, N., Bamler, R., Yague-Martinez, N., & Breit, H. (2009). Spaceborne spotlight SAR interferometry with TerraSAR-X. *IEEE Trans. Geosci. Remote Sens.*, *47*(5), 1524–1535. https://doi.org/10.1109/TGRS.2008.2004714

Eineder, M., Fritz, T., Abdel Jaber, W., Rossi, C., & Breit, H. (2012). Decadal Earth topography dynamics measured with TanDEM-X and SRTM. In *International Geoscience and Remote Sensing Symposium (IGARSS)* (pp. 1916–1919). https://doi.org/10.1109/IGARSS.2012.6351130

Frappart, F., Seyler, F., Martinez, J. M., León, J. G., & Cazenave, A. (2005). Floodplain water storage in the Negro River basin estimated from microwave remote sensing of inundation area and water levels. *Remote Sens. Environ.*, *99*(4), 387–399. https://doi.org/10.1016/j.rse.2005.08.016

Funk, C., Peterson, P., Landsfeld, M., Pedreros, D., Verdin, J., Shukla, S., … Michaelsen, J. (2015). The climate hazards infrared precipitation with stations — a new environmental record for monitoring extremes. *Scientific Data*, 1–21. https://doi.org/10.1038/sdata.2015.66

Gao, H., Birkett, C., & Lettenmaier, D. P. (2012). Global monitoring of large reservoir storage from satellite remote sensing. *Water Resources Research*, *48*(9), 1–12. https://doi.org/10.1029/2012WR012063

Glendenning, C. J., & Vervoort, R. W. (2010). Hydrological impacts of rainwater harvesting (RWH) in a case study catchment : The Arvari River , Rajasthan , India . Part 1 : Field-scale impacts. *Agricultural Water Management*, *98*(2), 331–342. https://doi.org/10.1016/j.agwat.2010.09.003

Glendenning, C. J., & Vervoort, R. W. (2011). Hydrological impacts of rainwater harvesting (RWH) in a case study catchment : The Arvari River , Rajasthan , India Part 2 . Catchment-scale impacts. *Agricultural Water Management*, *98*(4), 715–730. https://doi.org/10.1016/j.agwat.2010.11.010

Gorelick, N., Hancher, M., Dixon, M., Ilyushchenko, S., Thau, D., & Moore, R. (2017). Google

Earth Engine: Planetary-scale geospatial analysis for everyone. *Remote Sens. Environ.*, *202*, 18–27. https://doi.org/10.1016/j.rse.2017.06.031

Government of Tamil Nadu (2015). *Tamil Nadu State Action Plan for Climate Change*. Retrieved from http://www.environment.tn.nic.in/sapcc.html

Gunnell, Y., Anupama, K., & Sultan, B. (2007). Response of the South Indian runoff-harvesting civilization to northeast monsoon rainfall variability during the last 2000 years: Instrumental records and indirect evidence. *Holocene*, *17*(2), 207–215. https://doi.org/10.1177/0959683607075835

Gunnell, Y., & Krishnamurthy, A. (2003). Past and Present Status of Runoff Harvesting Systems in Dryland Peninsular India: A Critical Review. *Ambio*, *32*(4), 320–324.

Henry, J., Chastanet, P., Fellah, K., & Desnos, Y. (2006). Envisat multi-polarized ASAR data for flood mapping. *International Journal of Remote Sensing*, *27*(10), 1921–1929. https://doi.org/10.1080/01431160500486724

Hijioka, Y., Lin, E., Pereira, J., Corlett, R., Cui, X., Insarov, G., … Surjan, A. (2014). *Asia. Climate Change 2014: Impacts, Adaptation, and Vulnerability. Part B: Regional Aspects. Contribution of Working Group II to the Fifth Assessment Report of the Intergovernmental Panel on Climate Change*. Cambridge, United Kingdom and New York, NY, USA: Cambridge University Press.

Hong, S.-H., Wdowinski, S., Kim, S.-W., & Won, J.-S. (2010). Multi-temporal monitoring of wetland water levels in the Florida Everglades using interferometric synthetic aperture radar (InSAR). *Remote Sens. Environ.*, *114*(11), 2436–2447. https://doi.org/10.1016/j.rse.2010.05.019

Huang, C. (2018). Reviews of Geophysics Detecting, Extracting, and Monitoring Surface Water From Space Using Optical Sensors: A Review. *Reviews of Geophysics*, 333–360. https://doi.org/10.1029/2018RG000598

IPCC. (2014). *Climate Change 2014: Impacts, Adaptation, and Vulnerability. Part B: Regional Aspects. Contribution of Working Group II to the Fifth Assessment Report of the Intergovernmental Panel on Climate Change*. Cambridge, UK: Cambridge Univ Press.

Kajisa, K., Palanisami, K., & Sakurai, T. (2007). Effects on poverty and equity of the decline in collective tank irrigation management in Tamil Nadu , India. *Agricultural Economics*, *36*, 347–362.

Karmakar, N., Chakraborty, A., & Nanjundiah, R. S. (2017). Increased sporadic extremes decrease the intraseasonal variability in the Indian summer monsoon rainfall. *Scientific Reports*, *7*(7824), 1–7. https://doi.org/10.1038/s41598-017-07529-6

Karran, D. J., Westbrook, C. J., Wheaton, J. M., Johnston, C. A., & Bedard-haughn, A. (2017). Rapid surface-water volume estimations in beaver ponds. *Hydrology and Earth System Sciences*, *21*(352), 1039–1050. https://doi.org/10.5194/hess-21-1039-2017

Kasischke, E. S., Smith, K. B., Bourgeau-chavez, L. L., Romanowicz, E. A., Brunzell, S., & Richardson, C. J. (2003). Effects of seasonal hydrologic patterns in south Florida wetlands on radar backscatter measured from ERS-2 SAR imagery. *Remote Sensing of Environment*, *88*, 423–441. https://doi.org/10.1016/j.rse.2003.08.016

Kim, J. W. (2013). Applications of Synthetic Aperture Radar (SAR)/ SAR Interferometry (InSAR) for Monitoring of Wetland Water Level and Land Subsidence, (503).

Kumar, D., Patel, A., Ravindranath, R., & Singh, O. P. (2008). Chasing a Mirage: Water Harvesting and Artificial Recharge in Naturally Water-Scarce Regions. *Economic and Political Weekly*, *43*(35), 61–71. https://doi.org/10.2307/40278725

Kumar, D., & Rao, N. (2017). *Ecosystem Functions and Management* (Harpinder). Switzerland: Springer International Publishing AG. https://doi.org/10.1007/978-3-319-53967-6

Kumar, P., Wiltshire, A., Mathison, C., Asharaf, S., Ahrens, B., Lucas-Picher, P., … Jacob, D. (2013). Downscaled climate change projections with uncertainty assessment over India using a high resolution multi-model approach. *Science of the Total Environment*, *468–469*, S18–S30. https://doi.org/10.1016/j.scitotenv.2013.01.051

Kummu, M., Guillaume, J. H. A., Moel, H. De, Eisner, S., Flörke, M., & Porkka, M. (2016). The world's road to water scarcity: shortage and stress in the 20th century and pathways towards sustainability. *Scientific Reports*, *6*(38495), 1–16. https://doi.org/10.1038/srep38495

Kuo, C.-Y., & Kao, H.-C. (2011). Retracked Jason-2 Altimetry over Small Water Bodies: Case Study of Bajhang River, Taiwan. *Marine Geodesy*, *34*(March), 382–392. https://doi.org/10.1080/01490419.2011.584830

Lele, S., Srinivasan, V., Thomas, B. K., & Jamwal, P. (2018). Adapting to climate change in rapidly urbanizing river basins : insights from a multiple-concerns , multiple-stressors , and multi-level approach. *Water International*, *43*(2), 281–304. https://doi.org/10.1080/02508060.2017.1416442

Li, Q., & Gowing, J. (2005). A daily water balance modelling approach for simulating performance of tank-based irrigation systems. *Water Resources Management*, *19*(3), 211–231. https://doi.org/10.1007/s11269-005-2702-9

Liebe, J., Giesen, N. Van De, Andreini, M. S., Steenhuis, T. S., & Walter, M. T. (2009). Suitability and Limitations of ENVISAT ASAR for Monitoring Small Reservoirs in a Semiarid Area. *IEEE. Trans. Geosci. Remote Sens.*, *47*(5), 1536–1547.

Liebe, J., Van De Giesen, N., & Andreini, M. (2005). Estimation of small reservoir storage capacities in a semi-arid environment A case study in the Upper East Region of Ghana. *Phys. Chem. Earth*, *30*(6–7), 448–454. https://doi.org/10.1016/j.pce.2005.06.011

Liebe, J., Van De Giesen, N., Andreini, M., Walter, M. T., & Steenhuis, T. S. (2009). Determining watershed response in data poor environments with remotely sensed small reservoirs as runoff gauges. *Water Resources Research*, *45*(7), 1–12. https://doi.org/10.1029/2008WR007369

Magome, J., Ishidaira, H., & Takeuchi, K. (2003). Method for satellite monitoring of water storage in reservoirs for efficient regional water management. *Water Resour. Res.*, (2), 303–310.

Mall, R. K., Gupta, A., Singh, R., Singh, R. S., & Rathore, L. S. (2006). Water resources and climate change : An Indian perspective. *Arctic*, *90*(12), 1610–1626. https://doi.org/10.1016/S0143-8166(02)00004-0

Manjusree, P., Kumar, L. P., Bhatt, C. M., & Rao, G. S. (2012). Optimization of Threshold Ranges for Rapid Flood Inundation Mapping by Evaluating Backscatter Profiles of High Incidence Angle SAR Images, *3*(2), 113–122. https://doi.org/10.1007/s13753-012-0011-5

Mark, P. (2018). Radar Backscatter as a Function of Incidence Angle. Retrieved from http://satftp.soest.hawaii.edu/space/hawaii/vfts/kilauea/radar_ex/page2.html.

Martinis, S. (2010). *Automatic near real-time flood detection in high resolution X-band synthetic aperture radar satellite data using context-based classification on irregular graphs*. Retrieved from https://edoc.ub.uni-muenchen.de/12373/1/Martinis_Sandro.pdf

Martinis, S., & Plank, S. (2018). The Use of Sentinel-1 Time-Series Data to Improve Flood Monitoring in Arid Areas. *Remote Sens.*, *10*(583), 1–13. https://doi.org/10.3390/rs10040583

Matgen, P., Schumann, G., Henry, J., Hoffmann, L., & Pfister, L. (2007). Integration of SAR-

derived river inundation areas , high-precision topographic data and a river flow model toward near real-time flood management, *9*, 247–263. https://doi.org/10.1016/j.jag.2006.03.003

McCabe, M. F., Wood, E. F., Wójcik, R., Pan, M., Sheffield, J., Gao, H., & Su, H. (2008). Hydrological consistency using multi-sensor remote sensing data for water and energy cycle studies. *Remote Sensing of Environment*, *112*, 430–444. https://doi.org/10.1016/j.rse.2007.03.027

McCabe, M., Rodell, M., Alsdorf, D. E., Miralles, D. G., Uijlenhoet, R., Wagner, W., … Shi, J. (2017). The future of Earth observation in hydrology. *Hydrol. Earth Syst. Sci.*, *21*, 3879–3914.

McFeeters, S. K. (1996). The use of the Normalized Difference Water Index (NDWI) in the delineation of open water features. *Int J Remote Sens.*, *17*(7), 1425–1432. https://doi.org/10.1080/01431169608948714

Medina, C., Gomez-Enri, J., Alonso, J. J., & Villares, P. (2010). Water volume variations in Lake Izabal (Guatemala) from in situ measurements and ENVISAT Radar Altimeter (RA-2) and Advanced Synthetic Aperture Radar (ASAR) data products. *Journal of Hydrology*, *382*(1–4), 34–48. https://doi.org/10.1016/j.jhydrol.2009.12.016

Meigh, J. (1995). The impact of small farm reservoirs on urban water supplies in Botswana. In *Natural Resources Forum* (Vol. 19, pp. 71–83). Blackwell Publishing Ltd.

Mialhe, F., Gunnell, Y., & Mering, C. (2008). Synoptic assessment of water resource variability in reservoirs by remote sensing : General approach and application to the runoff harvesting systems of south India Franc. *Water Resour. Res.*, *44*, 1–14. https://doi.org/10.1029/2007WR006065

Minke, A. G., & Westbrook, C. J. (2010). Simplified Volume-Area-Depth Method for Estimating Water Storage of Prairie Potholes. *Wetlands*, *30*(3), 541–551. https://doi.org/10.1007/s13157-010-0044-8

Mosse, D. (2018). Colonial and Contemporary Ideologies of "Community Management": The Case of Tank Irrigation Development in South India. *Modern Asian Studies*, *33*(2), 303–338.

Moore, G. (1980). Satellite remote sensing of water turbidity. *Hydrological Sciences*, *25*(4), 407–421. https://doi.org/10.1080/02626668009491950

Mueller, N., Lewis, A., Roberts, D., Ring, S., Melrose, R., Sixsmith, J., … Ip, A. (2016). Water observations from space: Mapping surface water from 25years of Landsat imagery across Australia. *Remote Sens. Environ.*, *174*, 341–352. https://doi.org/10.1016/j.rse.2015.11.003

Musa, Z. N., Popescu, I., & Mynett, A. (2015). A review of applications of satellite SAR, optical, altimetry and DEM data for surface water modelling, mapping and parameter estimation. *Hydrol. Earth Syst. Sci.*, *12*(5), 4857–4878. https://doi.org/10.5194/hessd-12-4857-2015

Otsu, N. (1979). A Threshold Selection Method from Gray-Level Histograms. *IEEE Trans. Syst. Man Cybern.*, *9*(1), 62–66. https://doi.org/10.1109/TSMC.1979.4310076

Ottinger, M., Clauss, K., & Kuenzer, C. (2017). Large-Scale Assessment of Coastal Aquaculture Ponds with Sentinel-1 Time Series Data. *Remote Sens.*, *9*(440), 1–23. https://doi.org/10.3390/rs9050440

Ouma, Y. (2016). Evaluation of Multiresolution Digital Elevation Model (DEM) from Real-Time Kinematic GPS and Ancillary Data for Reservoir Storage Capacity Estimation. *Hydrology*, *3*(2), 16. https://doi.org/10.3390/hydrology3020016

Palanisami, A. K., Meinzen-dick, R., Giordano, M., Palanisami, K., Meinzen-dick, R., &

Giordano, M. (2010). Climate Change and Water Supplies : Options for Sustaining Tank Irrigation Potential in India. *Economic and Political Weekly*, *45*(26/27), 183–190.
Pandey, D. N., Gupta, A. K., & Anderson, D. M. (2003). Rainwater harvesting as an adaptation to climate change. *Current Science*, *85*(1), 46–59.
Pekel, J.-F., Cottam, A., Gorelick, N., & Belward, A. S. (2016). High-resolution mapping of global surface water and its long-term changes. *Nature*, *540*(7633), 418–422. https://doi.org/10.1038/nature20584
Peng, D., Guo, S., Liu, P., & Liu, T. (2006). Reservoir Storage Curve Estimation Based on Remote Sensing Data. *Journal of Hydrologic Engineering*, *11*(2), 165–172. https://doi.org/10.1061/(ASCE)1084-0699(2006)11:2(165)
Rizzoli, P., Martone, M., Gonzalez, C., Wecklich, C., Tridon, D. B., Bräutigam, B., … Moreira, A. (2017). ISPRS Journal of Photogrammetry and Remote Sensing Generation and performance assessment of the global TanDEM-X digital elevation model. *ISPRS Journal of Photogrammetry and Remote Sensing*, *132*, 119–139. https://doi.org/10.1016/j.isprsjprs.2017.08.008
Rodrigues, L. N., & Liebe, J. (2013). Small reservoirs depth-area-volume relationships in Savannah Regions of Brazil and Ghana. *Water Resources and Irrigation Management*, *1*, 1–10.
Rossi, C., Gonzalez, F. R., Fritz, T., Yague-martinez, N., & Eineder, M. (2012). TanDEM-X calibrated Raw DEM generation. *ISPRS Journal of Photogrammetry and Remote Sensing*, *73*, 12–20. https://doi.org/10.1016/j.isprsjprs.2012.05.014
Sakthivadivel, R., Fernando, N., & Brewer, J. D. (1997). *Rehabilitation planning for small tanks in cascades: A methodology based on rapid assessment*. *International Irrigation Management Institute*. Colombo, Sri Lanka. https://doi.org/http://dx.doi.org/10.3910/2009.011
Santos, J., Silva, D., Seyler, F., Calmant, S., Corrêa, O., Filho, R., … Calmant, S. (2012). Water level dynamics of Amazon wetlands at the watershed scale by satellite altimetry. *Int J Remote Sens*, *33*(22), 3323–3353. https://doi.org/10.1080/01431161.2010.531914
Sato, T. (2013). Beyond water-intensive agriculture: Expansion of Prosopis juliflora and its growing economic use in Tamil Nadu, India. *Land Use Policy*, *35*, 283–292. https://doi.org/10.1016/j.landusepol.2013.06.001
Sato, T. (2017). Livelihood Transformability in Indian Villages with Poor Water Resources : The Case of Tamil Nadu. *Senri Ethological Studies*, *96*, 47–61.
Sawunyama, T., Senzanje, A., & Mhizha, A. (2006). Estimation of small reservoir storage capacities in Limpopo River Basin using geographical information systems (GIS) and remotely sensed surface areas: Case of Mzingwane catchment. *Physics and Chemistry of the Earth. Chem. Earth*, *31*(15–16), 935–943. https://doi.org/10.1016/j.pce.2006.08.008
Shah, T. (2004). Water and Welfare: Critical Issues in India's Water Future. *Economic and Political Weekly*, *39*(12), 1211–1213.
Shah, T. (2009). Climate change and groundwater : India's opportunities for mitigation and adaptation. *Environmental Research Letters*, *4*, 1–13. https://doi.org/10.1088/1748-9326/4/3/035005
Shiklomanov, I. A. (2000). Appraisal and Assessment of World Water Resources. *Water International*, *25*(1), 10–32. https://doi.org/10.1080/02508060008686794
Siderius, C., Boonstra, H., Munaswamy, V., Ramana, C., Kabat, P., van Ierland, E., & Hellegers, P. (2015). Climate-smart tank irrigation: A multi-year analysis of improved conjunctive

water use under high rainfall variability. *Agricultural Water Management*, *148*, 52–62. https://doi.org/10.1016/j.agwat.2014.09.009

Sishodia, R. P., Shukla, S., Graham, W. D., Wani, S. P., & Garg, K. K. (2016). Journal of Hydrology : Regional Studies Bi-decadal groundwater level trends in a semi-arid south indian region : Declines , causes and management. *Biochemical Pharmacology*, *8*, 43–58. https://doi.org/10.1016/j.ejrh.2016.09.005

Srivastava, R., Kannan, K., Mohanty, R., Nanda, P., Sahoo, N., Mohanty, R., & Das, M. (2009). Rainwater Management for Smallholder Irrigation and it's Impact on Crop Yields in Eastern India. *Water Resour. Manage.*, *23*, 1237–1255. https://doi.org/10.1007/s11269-008-9324-y

Tholey, N., Clandillon, S., & Fraipont, P. D. E. (1997). The contribution of spaceborne SAR and optical data in monitoring flood events: examples in northern and southern France. *Hydrological Processes*, *11*(10), 1409–1413.

Twele, A., Cao, W., Plank, S., Martinis, S., Cao, W., & Plank, S. (2016). Sentinel-1-based flood mapping : a fully automated processing chain. *Int J Remote Sens*, *37*(13), 2990–3004. https://doi.org/10.1080/01431161.2016.1192304

Van Meter, K. J., Steiff, M., McLaughlin, D. L., & Basu, N. B. (2016). The socioecohydrology of rainwater harvesting in India: Understanding water storage and release dynamics across spatial scales. *Hydrol. Earth Syst. Sci.*, *20*(7), 2629–2647. https://doi.org/10.5194/hess-20-2629-2016

Vaze, J., Teng, J., & Spencer, G. (2010). Impact of DEM accuracy and resolution on topographic indices. *Environmental Modelling and Software*, *25*(10), 1086–1098. https://doi.org/10.1016/j.envsoft.2010.03.014

Venkatesan, V., Balamurugan, R., & Krishnaveni, M. (2011). Establishing water surface area-storage capacity relationship of small tanks using SRTM and GPS. *Energy Procedia*, *16*(PART B), 1167–1173. https://doi.org/10.1016/j.egypro.2012.01.186

Verpoorter, C., Kutser, T., Seekell, D. A., & Tranvik, L. J. (2014). A global inventory of lakes based on high-resolution satellite imagery. *Geophys. Res. Lett*, *41*, 6396–6402. https://doi.org/10.1002/2014GL060641.Received

Vorosmarty, C. J., Green, P., Salisbury, J., & Lammers, R. B. (2000). Global Water Resources: Vulnerability from Climate Change and Population Growth. *Science*, *289*(5477), 284–289. https://doi.org/10.1126/science.289.5477.284

Wada, Y., Van Beek, L. P. H., Van Kempen, C. M., Reckman, J. W. T. M., Vasak, S., & Bierkens, M. F. P. (2010). Global depletion of groundwater resources. *Geophys. Res. Lett*, *37*(20), 1–5. https://doi.org/10.1029/2010GL044571

Wendleder, A., Wessel, B., Roth, A., Breunig, M., Martin, K., & Wagenbrenner, S. (2013). TanDEM-X Water Indication Mask: Generation and First Evaluation Results. *J-STARS*, *6*(1), 171–179.

Wiltshire, A., Gornall, J., Booth, B., Dennis, E., Falloon, P., Kay, G., … Betts, R. (2013). The importance of population, climate change and CO2 plant physiological forcing in determining future global water stress. *Global Environmental Change*, *23*(5), 1083–1097. https://doi.org/10.1016/j.gloenvcha.2013.06.005

Xie, C., Xu, J., Shao, Y., Cui, B., Goel, K., Zhang, Y., & Yuan, M. (2015). Long term detection of water depth changes of coastal wetlands in the Yellow River Delta based on distributed scatterer interferometry. *Remote Sens. Environ.*, *164*, 238–253. https://doi.org/10.1016/j.rse.2015.04.010

Young, S., Peschel, J., Penny, G., Thompson, S., & Srinivasan, V. (2017). Robot-Assisted Measurement for Hydrologic Understanding in Data Sparse Regions. *Water*, *9*(7), 494. https://doi.org/10.3390/w9070494

Zeng, L., Schmitt, M., Li, L., Zhu, X. X., & Li, L. (2017). Analysing changes of the Poyang Lake water area using Sentinel-1 synthetic aperture radar imagery Analysing changes of the Poyang Lake water area using Sentinel-1 synthetic aperture radar imagery. *Int J Remote Sens*, *38*(23), 7041–7069. https://doi.org/10.1080/01431161.2017.1370151

Zhang, S., Foerster, S., Medeiros, P., Carlos, J., Araújo, D., Motagh, M., & Waske, B. (2016). Bathymetric survey of water reservoirs in north-eastern Brazil based on TanDEM-X satellite data. *Sci Total Environ.*, *571*, 575–593. https://doi.org/10.1016/j.scitotenv.2016.07.024

Appendix A: Field photos

Figure A1: Topographic field survey in July 2016 using total station when tanks contained no water.

Figure A2: Invasive vegetation in tank bed highlighted tank state of disrepair.

Figure A3: Tank with water highlighted high water turbidity.

Appendix B: DEM comparison

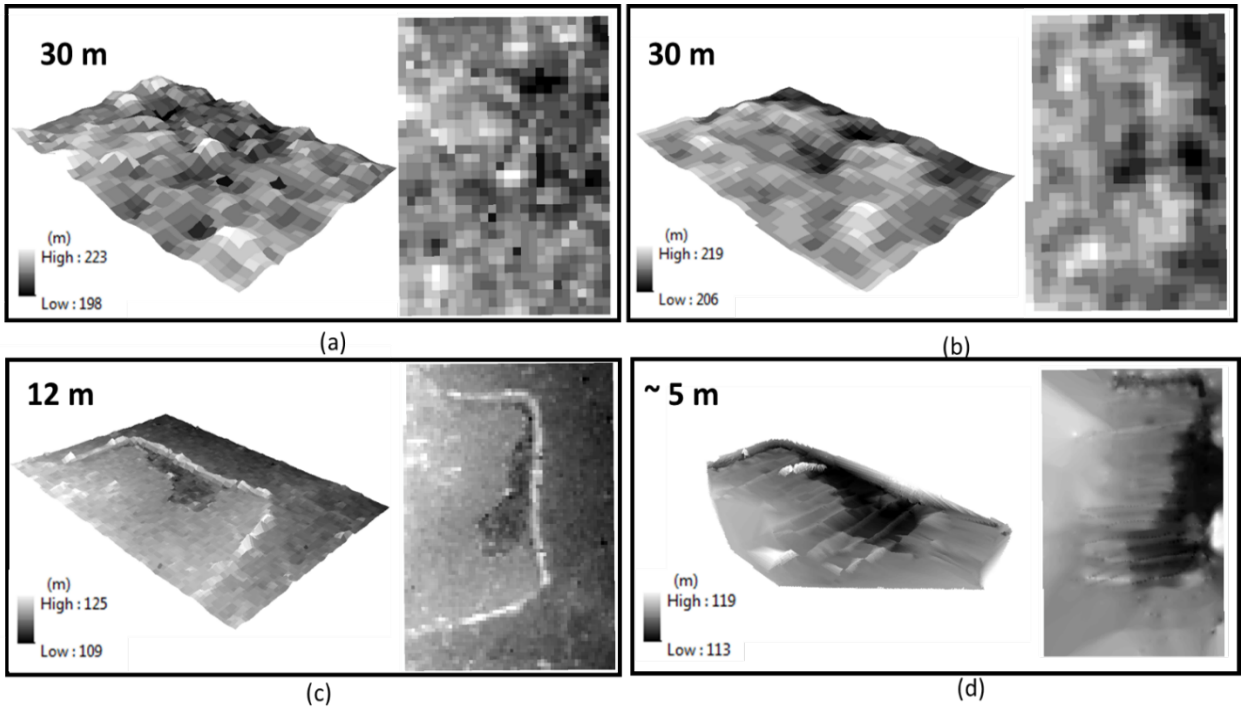

Figure B1: DEM comparison for tank geometry. (a) 30 m STRM DEM, (b) 30 m ASTER DEM, (c) TanDEM-X 12 m DEM, and (d) field interpolated topographic data DEM.

Appendix C: SAR missions- Past, current, future

Table C1: Past, Current and Future SAR Missions

Satellite Name (sponsor)	Lifespan		Specifications				
			frequency	polarization modes	spatial res. (m)	swath width (km)	repeat cycle (d)
SAOCOM (CONAE)	2018	Current	L-band	single pol. (HH,VV,HV,VH), dual pol. (VV/VH,HH/HV), quad pol.	10 - 100m	30 - 350	16
Gaofen-3 (CNSA)	2016	Current	C-band	single pol. (HH,VV,HV,VH), dual pol. (VV/VH,HH/HV)	1-500	650	29
KOMPSAT-5	2013	Current	X-Band	single pol. (HH,VV,HV,VH)	1-20	5-100	28
Sentinel 1 (ESA)	2014	Current	C-band	dual pol. (VV/VH,HH/HV)	5-40	20- 400	12
RADARSAT Constellation (CSA/ MDA)	2019	Current	C-band	single pol. (HH,VV,HV,VH), dual pol. (VV/VH,HH/HV), quad pol.	3-100	5-500	12
ALOS PALSAR-2 (JAXA)	2013	Current	L-band	single pol. (HH,VV), dual pol. (HH/HV, VV/VH), quad, compact pol.	1-100	25-350	14
TerraSAR-X (DLR)	2007	Current	X-Band	single pol. (HH,VV,HV,VH), dual pol. (HH/VV, HH/HV, VV/VH)	1-18	10-1650	11
COSMO- SkyMed (ASI)	2007	Current	X-Band	single pol. (HH,VV,HV,VH), dual pol. (HH/VV, HH/HV, VV/VH)	1-100	10-200	16
ERS-2 (ESA)	1995	2011	C-band	single pol. (VV)	30	100	35
ENVISAT ASAR (ESA)	2002	2012	C-band	single pol. (HH,VV,HV,VH),	30-500	5-400	35
RADARSAT 1 (CSA/ MDA)	1995	2013	C-band	single pol. (HH)	8-100	50-500	24
RADARSAT 2 (CSA/ MDA)	2007	Current	C-band	single pol. (HH,VV,HV,VH), dual pol. (VV/VH,HH/HV), quad pol.	3-100	20-500	24
ALOS- PALSAR (JAXA)	2006	2011	L-Band	single pol. (HH,VV), dual pol. (HH/HV, VV/VH), quad pol.	10-100	30-350	46

Appendix D: Deriving the power function out of the linear line from the log-log curves

Figure D1 provides a schematic of the process to retrieve Equation (3.1) - the V-A power equation. The minimum (h_{min}) and maximum topographic elevation (h_{max}) was extracted for each tank. Using a surface volume tool, the surface water extent and the volume was calculated for 0.05 m increments from h_{min} to h_{max} (3 m max.).

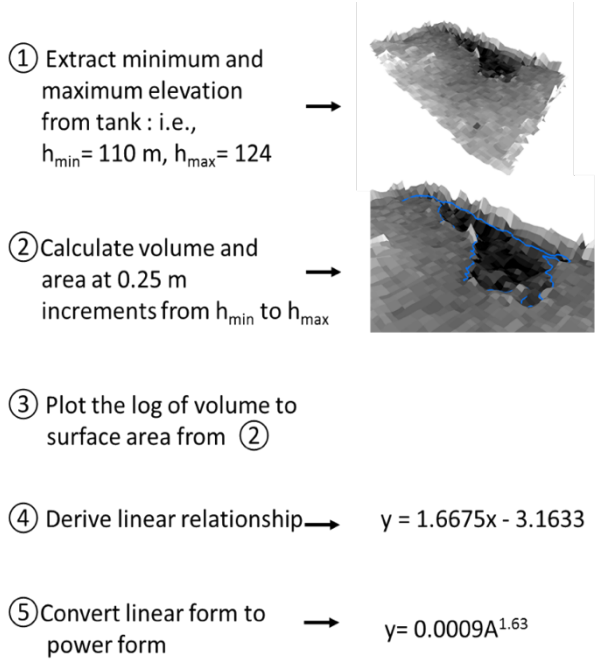

Figure D1: Process to retrieve power V-A relationship. Example provided specific to Tank 1.

Appendix D Continued

To derive the V-A relations to the power equation, it was necessary to determine the linear regression equations for the logarithms of surface area and volume. The output from the surface volume analysis allowed the creation of a log area log volume curve for each tank. Using the log-log curve it was possible to make a linear line that represents the relationship. The function of the linear line was rewritten to a power function using basic logarithm principles. Figure D2 provides an example of deriving the power function for Tank 1 using the linear regression equation from the log area-log volume curve. The derived power function represents the V-A relationship. When iterating this process for each tank, the result was 72 different V-A relationships with 72 unique a and b parameters.

Wanted power function:

$y = k * A^{a}$

Linear function of log Area – log Volume:

$y = 1.6675 * x - 3.1633$

Logarithmic principle:

$y = m * x + b$

$\log_{10}(y) = a * (\log_{10}(x)) + \log_{10}(k)$

$m = a$

$X = \log_{10}(x)$

$b = \log_{10}(k)$

$y = \log_{10}(y)$

Calculation:

$b = \log_{10}(k) = -3.1633$

$k = 10^{b} = 10^{-3.1633} = 0.0007$

$m = a$

$a = m = 1.6775$

Resulting power function:

$V = 0.0007 * A^{1.6775}$

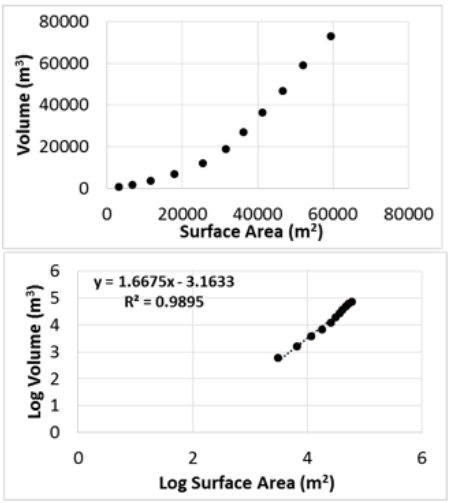

Figure D2: Example of process to retrieve power form of linear log area-log volume equation for Tank 1.

Appendix E: Maximum water extent monitoring

Figure E1 displays 12 SAR scenes for eight tanks in the upper basin. To extract maximum SW extent, SW extent was extracted from each date for each tank. Tank mask boundaries were used to extract tank regions. From the time-series of SW estimates, the maximum SW extent was used in the volume estimates at the basin scale. This was completed for two monsoon seasons (2015 and 2017).

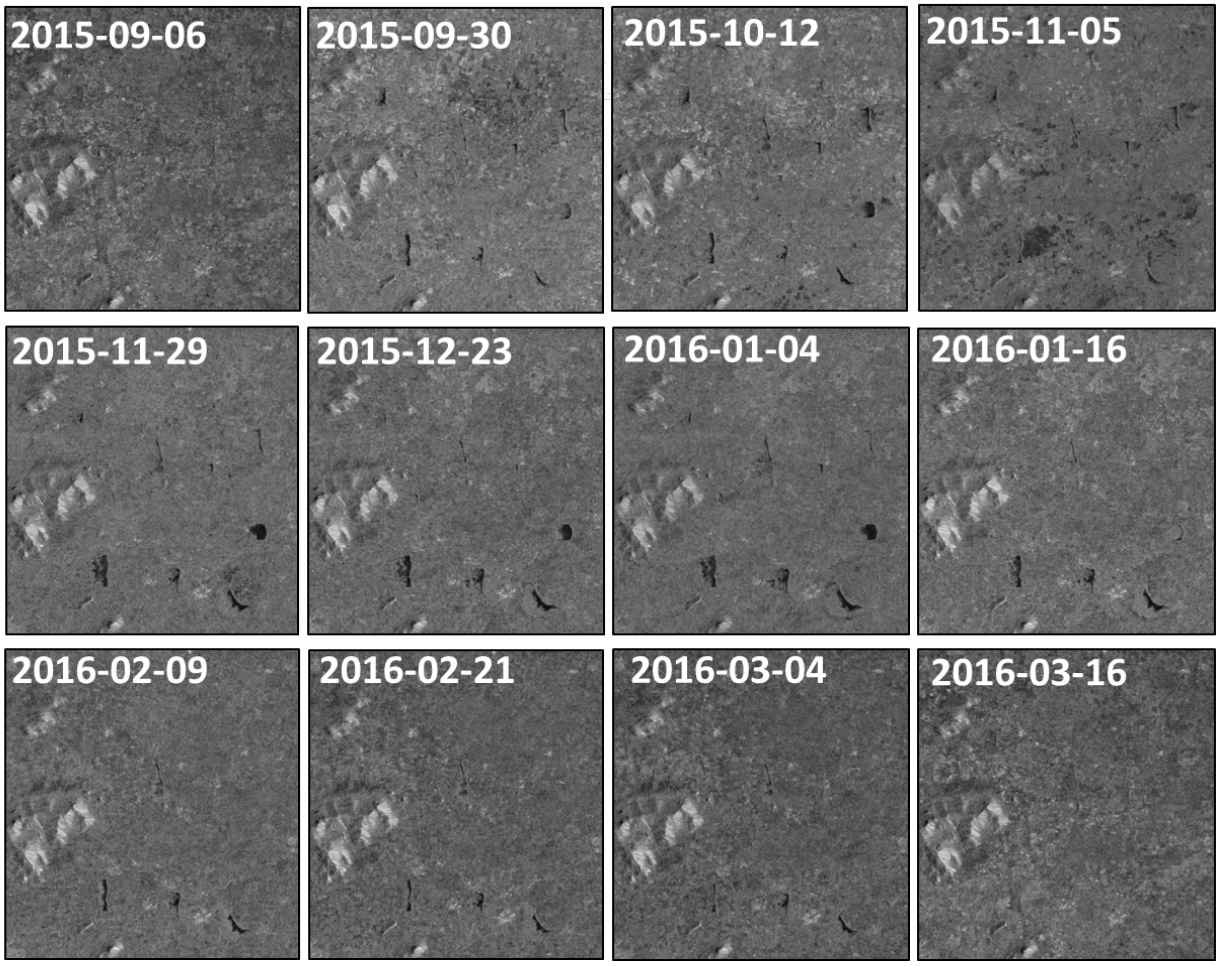

Figure E1: Time series of SAR S1-A scenes over the 2015-2016 monsoon season for eight tanks in the upper basin.

Appendix F: SAR water delineation – VV versus VH

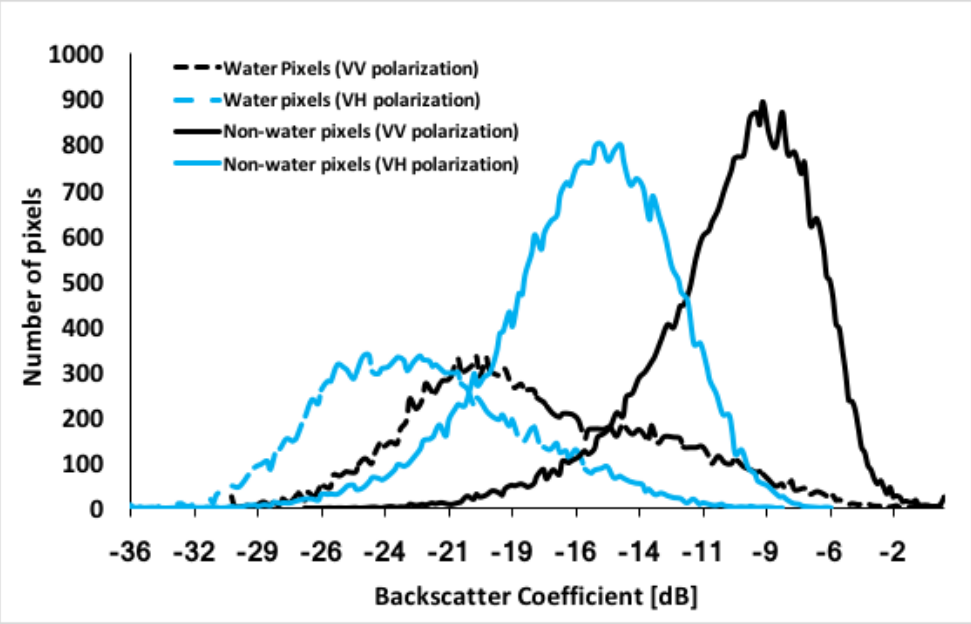

Figure F1: For SW delineated with PS, histograms of the water and non-water pixels for the SAR backscatter coefficients in VH and VV polarizations.

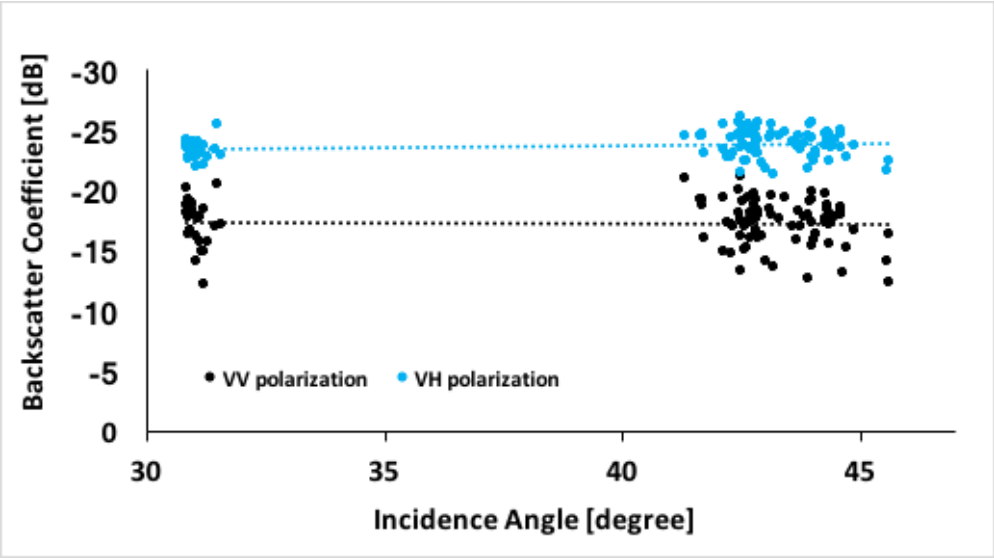

Figure F2: The SAR backscatter coefficients (VH and VV polarizations) from the S1-A as a function of the incidence angle over water bodies. The linear regression lines are also plotted.